Carbon Budgets in Northwestern Gulf of Mexico Coastal Estuaries

Hongming Yao[1,*#], Paul A. Montagna[2], Michael S. Wetz[2], Cory J. Staryk[1,2], and Xinping Hu[1,2]

[1]Department of Physical and Environmental Sciences, Texas A&M University-Corpus Christi, Texas 78412, United States

[2]Harte Research Institute for Gulf of Mexico Studies, Texas A&M University-Corpus Christi, Texas 78412, United States

[*]Corresponding author:
Hongming Yao (hm.yao@siat.ac.cn)

Current address:
Shenzhen Engineering Laboratory of Ocean Environmental Big Data Analysis and Application, Shenzhen Institute of Advanced Technology, Chinese Academy of Sciences, Shenzhen 518055, China

Key Points:

- Lateral exchanges between tidal wetlands and estuaries account for 97.9% and 84.4% of organic and inorganic carbon inputs.
- Air-water CO_2 flux is 16.8 ± 3.0 mol·C·m^{-2}·yr^{-1}, a moderate CO_2 source to the atmosphere compared with all North American estuaries.
- Carbon fluxes in the northwestern Gulf of Mexico are highly variable due to an extreme range of hydrologic conditions from drought to flooding.

Abstract

As coastal areas become more vulnerable to climatic impacts, the need for understanding estuarine carbon budgets with sufficient spatiotemporal resolution arises. A mass balance model has been constructed for carbon fluxes in four estuaries along the northwestern Gulf of Mexico (nwGOM) coast from 2014 to 2018. The annual lateral carbon exports from tidal marsh-mangrove to estuaries account for 97.9% and 84.4% of total organic carbon (TOC) and dissolved inorganic carbon (DIC) inputs, respectively. This sustains a relatively high air-water CO_2 flux (16.8 ± 3.0 $mol\cdot C\cdot m^{-2}\cdot yr^{-1}$) compared with most estuaries on the North American Atlantic coast. In addition, annual air-water CO_2 flux reaches as high as oceanic DIC export coastwide. The majority of imported riverine TOC has been exported to the coastal ocean (62.2%), leaving 22.3% of TOC for sediment deposition and 15.5% for remineralization. These fluxes are highly variable because of hydrologic variability. For example, episodic flooding can elevate estuarine CO_2 efflux by 2 – 10 times in short periods of time. Flood following a drought state also increases lateral exchanges of TOC (from 90.7 ± 65.7 to 200.5 ± 160.2 $mmol\cdot C\cdot m^{-2}\cdot d^{-1}$) and DIC (from 49.1 ± 39.8 to 166.9 ± 236.1 $mmol\cdot C\cdot m^{-2}\cdot d^{-1}$). The contribution of nwGOM estuaries increases the overall North American estuarine CO_2 flux by 220%, impacting coastal carbon budget. Hydrologic control explains temporal variability in these estimates.

1 Introduction

Coastal areas consisting of tidal wetlands and estuaries play a key role in the global carbon cycle. Estuaries are highly dynamic, receiving terrestrial carbon from rivers and surrounding watersheds, which can be exported in various forms to the coastal ocean. For example, estuaries account for only 0.3% (1.05×10^{12} m^2) surface area of the global ocean, yet CO_2 emission, estimated at 0.10 – 0.25 $Pg\cdot C\cdot yr^{-1}$ in estuaries (Cai, 2011; Chen et al., 2013), is equivalent to the magnitude of continental shelves CO_2 uptake and 30% of riverine total carbon input (Bauer et al., 2013; Cai, 2011). However, the uniqueness of each estuary from geomorphological, climatic, and hydrologic perspectives results in spatiotemporal heterogeneity in carbon processing across the world (Bauer et al., 2013; Montagna et al., 2013). In addition, anthropogenic effects vary spatially because of land-use change, wastewater discharge, water diversions, etc., and these effects have increased terrestrial total carbon influx to estuaries by 25% globally since the pre-industrial times, from 0.8 to 1.0 $Pg\cdot C\cdot yr^{-1}$ (Regnier et al., 2013). Attempts to synthesize estuarine carbon budgets face several challenges, e.g., identifying each C-involved biogeochemical process including ecosystem metabolism (NEM), riverine discharge, lateral exchange—from tidal wetland via tidal or submarine groundwater discharge (SGD), air-water CO_2 flux, export to the coastal ocean, and burial in sediment, and determining sufficient resolution for a variety of research in terms of temporal and spatial scales (Swaney et al., 2012). NEM in the water column and sediment and air-water CO_2 flux are critical for understanding the connection between organic and inorganic carbon fluxes in an estuary. However, the presence of large variability requires better spatiotemporal assessment of average NEM in order to obtain more accurate estuarine carbon budgets.

Carbon fluxes can be estimated in several different ways. Process-based models that couple estuarine hydrodynamics and biogeochemistry can link organic and inorganic carbon cycles (Gordon et al., 1996; Laruelle et al., 2017). However, detailed information at fine spatial and temporal scales is required to constrain potential errors in these models (Bauer et al., 2013; Kemp et al., 1997). On the other hand, mass balance approaches based on observations and stoichiometric relationships may amplify uncertainties because of the propagation of errors (Smith et al., 1991). However, models based on the latter approach are capable of separating individual processes that significantly influence the regional carbon cycle, and errors could be constrained or at least recognized if temporal and spatial patterns are chosen carefully (Maher & Eyre, 2012).

There are few carbon budget estimates in subtropical estuaries worldwide (Crosswell et al., 2017; Laruelle et al., 2017; Maher & Eyre, 2012). The Gulf of Mexico (GOM) has the world's largest lagoonal estuary (Laguna Madre of Texas and Mexico) and many other smaller lagoonal estuaries (Dürr et al., 2011), i.e., estuaries that are separated from the coastal ocean by barrier islands, through which channels and waterways connect the water bodies. Even though rivers in this region are rich in inorganic carbon (Stets et al., 2014; Zeng et al., 2011), it is difficult to quantify carbon flows because of high spatiotemporal variability. On the northwestern Gulf of Mexico (nwGOM) coast, river flow decreases sharply from northeast to southwest, which is one of the most distinctive hydrologic features in this area (Montagna et al., 2013). Dam construction and river fragmentation (Murgulet et al., 2016) and climatic fluctuations between drought and flooding periods (Yao & Hu, 2017; Yao et al., 2020) further alter and drive the hydrologic conditions of this region.

The objectives of this study were to: 1) construct detailed carbon budgets for nwGOM estuaries using a mass balance model based on bi-weekly to quarterly observations, 2) examine different biogeochemical drivers for several processes (riverine inflow, lateral exchange, burial, air-water CO_2 flux, NEM, export to the ocean), and 3) assess climatic impact on the estuarine carbon budget, including short-term episodic flooding and long-term sea level rise.

2 Methods

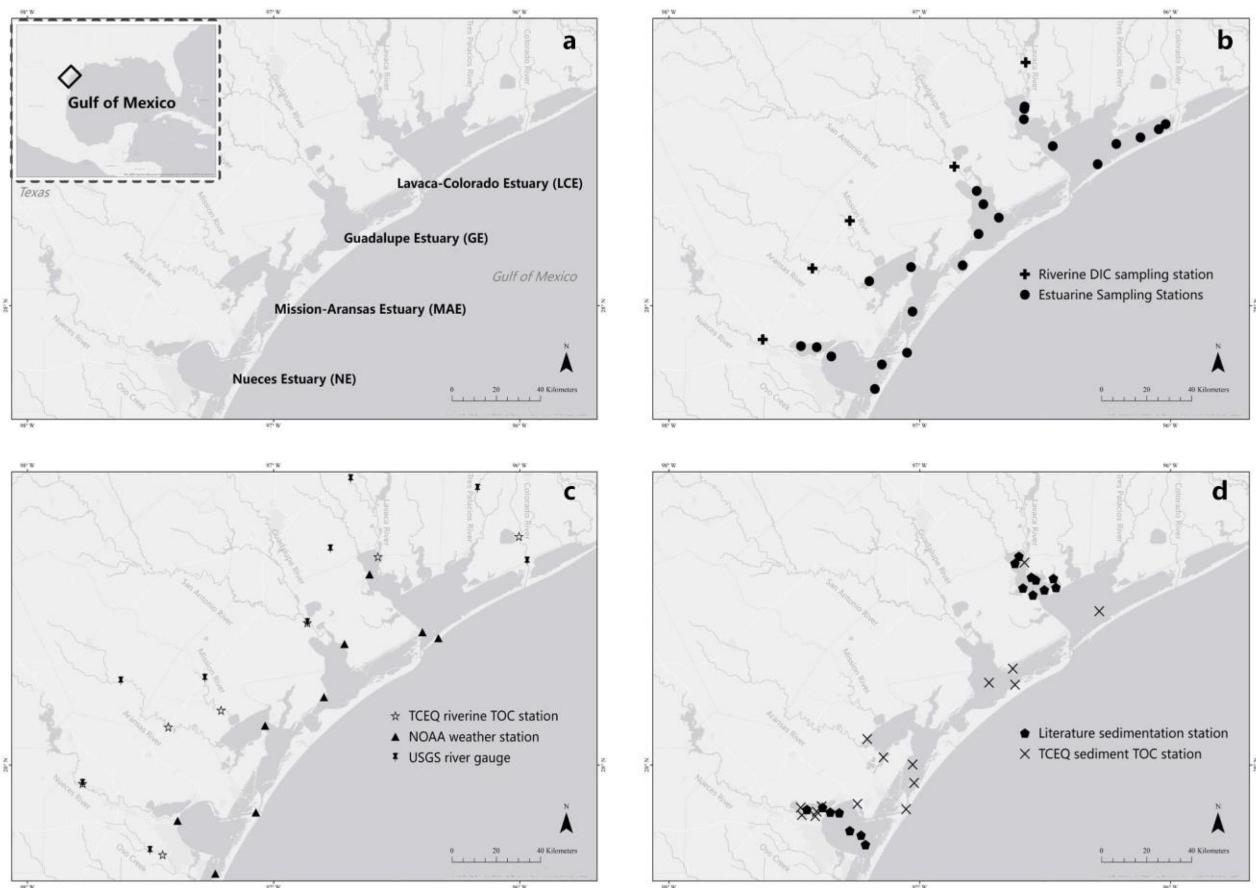

Figure 1. Northwestern GOM estuaries. **a**, nwGOM estuaries names and locations. **b**, water column sampling stations. **c**, riverine and weather stations used in data interpretation. **d**, sedimentation stations used in data interpretation.

2.1 Study sites

Four nwGOM estuaries (Fig. 1a) — Lavaca-Colorado Estuary (LCE), Guadalupe Estuary (GE), Mission-Aransas Estuary (MAE), and Nueces Estuary (NE) — were studied from April

2014 to April 2018. Hurricane Harvey made landfall close to the southern end of this coastal area in August 2017. Average depth of these microtidal estuaries was approximately 1 m (Table 1), and these estuaries have restricted connections to the GOM due to the presence of barrier islands (Fig. 1; Table 1). Each estuary receives input from one or two rivers. We designated the upper estuary as the area subject to more freshwater influence from rivers, whereas the lower estuary represents the area connected with the GOM through a tidal inlet. The only exception was GE, which is river inflow-dominated due to its limited tidal exchange (Fig. 1) (Montagna & Kalke, 1992). The Texas coastline was ideal to assess the effects of spatiotemporal variability on the estuarine carbon cycle because of its geomorphological similarity and differences in hydrology (Table 1).

2.2 Field sampling and laboratory analyses

Field campaigns on different time intervals were conducted (Table S1), both surface (0.1 m) and bottom samples (about 0.1 m above the bottom sediment) were taken. *In-situ* data, including temperature, depth, etc., were acquired by a calibrated YSI 6600 V2 data sonde. Dissolved inorganic carbon (DIC) was determined by acidifying 0.5 mL samples with 10% phosphoric acid and the extracted CO_2 was quantified on an AS-C3 DIC analyzer (Apollo SciTech), all DIC samples were analyzed against Certified Reference Materials (Batch#142, 156, 159, Dickson & Anderson 2003) with a precision of ± 0.1%. pH was measured using spectrophotometric method of purified m-cresol purple for samples (salinity ≥ 20, with ± 0.0004 precision; Carter et al., 2013), or an Orion™ Ross pH electrode (salinity < 20, ± 0.01 precision). The pH electrode was calibrated using NBS buffers (4.01, 7.00, 10.01). All pH measurements were done at 25 ± 0.1 °C, and the lab measured pH values were converted to the total scale at *in-situ* temperature using the program CO2SYS (MatLab® version) using measured pH and DIC. Salinity was measured using a benchtop salinometer calibrated with MilliQ water and known salinity Certified Reference Material (Batch#142, 156, 159). Ca^{2+} was titrated by egtazic acid (EGTA) on a Metrohm 888 Titrando automatic titrator using a calcium ion selective electrode to detect endpoint (Kanamori & Ikegami, 1980), and the precision was ± 0.2 %. Water TOC samples were analyzed using the High Temperature Catalytic Oxidation method on a Shimadzu TOC-Vs analyzer (Wetz et al., 2017).

2.3 Carbon mass balance

The major carbon fluxes in an estuary involve multiple processes, including riverine input F_{Rv}, lateral exchange F_L (i.e., exchange between tidal wetlands and estuaries via tidal activities and SGD; Maher et al., 2018; Najjar et al., 2017), net ecosystem metabolism (NEM) F_{NEM}, air-water CO_2 flux F_{CO2}, carbon deposition due to precipitation F_P, oceanic export F_{Ex} (i.e. net export after budgeting exchanging and residual flows between estuary and the coastal ocean), sedimentation F_D and calcification F_{Ca} (Crosswell et al., 2017; Laruelle et al., 2017; Maher & Eyre, 2012; Najjar et al., 2018). Because these estuaries are a net CO_2 source to the atmosphere (Yao et al. 2020), the steady-state mass balance equation for estuarine DIC would be:

$$F_{Rv-DIC} + F_{L-DIC} + F_{P-DIC} = F_{NEM} + F_{CO2} + F_{Ca} + F_{Ex-DIC} \quad (1)$$

F_{NEM} is negative for heterotrophy and positive if it is autotrophy. For total organic carbon (TOC), which consists of dissolved organic carbon (DOC) and particulate organic carbon (POC), the steady-state equation can be written as:

$$F_{Rv-TOC} + F_{L-TOC} + F_{P-TOC} + F_{NEM} = F_D + F_{Ex-TOC} \quad (2)$$

Note that all budget terms are estimated independently except for lateral exchange, which is calculated as residual from the mass balance.

2.4 Riverine input (F_{Rv})

Riverine carbon fluxes (F_{Rv}, µmol·C·d^{-1}) were estimated from riverine DIC or TOC (C_{Rv}, µmol·C·kg^{-1}), daily average discharge in each month (V_{Rv}, m^3·d^{-1}; Table 1) and water density (ρ, kg·m^{-3}):

$$F_{Rv} = C_{Rv} \times V_{Rv} \times \rho \quad (3)$$

where riverine DIC was from our river mouth surveys every other month between October 2015 and May 2018 (see Fig. 1b for station information; Table 1 for averaged endmember values; Table S1 for schedule details), historical riverine TOC data (1969 – 2018) were retrieved from the Surface Water Quality Monitoring Program of Texas Commission on Environmental Quality (TCEQ; https://www.tceq.texas.gov/waterquality/monitoring/index.html). Average riverine DIC and TOC were derived from dry and wet conditions (values in Table 1, hydrologic condition division in Table 4), respectively. Cumulative monthly discharges were obtained from gauges of the U.S. Geological Survey (USGS; https://waterdata.usgs.gov/tx/nwis/rt) (Fig.1c; Table 1).

2.5 Precipitation (F_P)

Carbon deposition through precipitation was assessed by atmospheric TOC and DIC, respectively. Regional atmospheric POC deposition was small enough to be ignored (0.1 – 1.3×10^{-3} µmol·C·L^{-1} , Benway & Coble, 2014). Average atmospheric DOC (161 µmol·C·L^{-1}) and DIC (17 µmol·C·L^{-1}; Willey et al., 2000) were applied in conjunction with monthly precipitation rates (Texas Water Development Board, TWDB, http://www.twdb.texas.gov/) to estimate rainfall input of carbon to these estuaries.

2.6 Air-water CO2 flux (FCO2)

Air-water CO_2 flux (F_{CO2}; mmol·C·m^{-2}·d^{-1}) in each station of each campaign was calculated:

$$F_{CO2} = k \cdot \mathrm{K}_0(p\mathrm{CO}_{2,\mathrm{water}} - p\mathrm{CO}_{2,\mathrm{air}}) \quad (4)$$

where K_0 is solubility coefficient related to temperature and salinity (mol·C·m^{-3}·Pa^{-1}; Weiss, 1974), *k* is the gas transfer velocity that was derived from wind speed at 10 m height (cm·h^{-1}; Jiang et al., 2008) and $pCO_{2,air}$ (μatm) was calculated as $pCO_{2,air} = xCO_{2,air} \times (P_b - P_w)$. P_b (atm) is the barometric pressure from NOAA weather stations (Fig. 1c), P_w (atm) is water vapor pressure calculated using salinity and temperature (Weiss and Price 1980), and $xCO_{2,air}$ (ppm) is the mole fraction of atmospheric CO_2 in dry air monitored by NOAA (https://www.pmel.noaa.gov/co2/story/Coastal+MS). Wind speed was obtained from NOAA coastal weather station and converted to 10 m height (https://tidesandcurrents.noaa.gov/map/index.html?type=met&region=Texas; Fig. 1c). $pCO_{2,water}$ (μatm) was calculated using measured DIC (± 0.1%) and pH (± 0.0004 or ±0.01depending on the analytical method used) as the input variables and the program CO2SYS. Carbonic acid dissociation constants (K_1, K_2) were from Millero (2010) and the bisulfate dissociation constant was from Dickson (1990). Paired DIC/pH as the input variables in CO2SYS could introduce 2.6 – 3.2 % uncertainty for calculated pCO_2 (Orr et al., 2018), which was approximately ± 8 – 16 μatm in this study (by applying annual average pCO_2 range from those estuaries). Calculated $pCO_{2,water}$ values were in good agreement with *in-situ* monitored $pCO_{2,water}$ (± 20 μatm; Yao et al., 2020). A positive F_{CO2} indicated CO_2 emission from water, and negative value represented CO_2 uptake by water.

2.7 Net ecosystem metabolism (F_{NEM})

Because mixed layer benthic and pelagic metabolic processes would generate/consume CO_2 and influence F_{CO2} directly, NEM was estimated using a linear regression equation (mmol·C·m^{-2}·d^{-1}; Eq. 5) that was derived by Maher & Eyre (2012), who found a significant inverse relationship ($R^2 = 0.898$, $p < 0.001$) between F_{CO2} and F_{NEM} based on data from twelve estuaries worldwide. Furthermore, Laruelle et al. (2013) applied this equation to estimate another 68 estuarine F_{CO2} globally and found a ~26.8% difference by comparing direct observations of CO_2 flux and NEM-derived estimates for lagoonal estuaries.

$$F_{CO2} = -0.4236 \times F_{NEM} + 11.991 \qquad (5)$$

2.8 Sediment deposition (F_D)

Sediment deposition flux (F_D; mmol·C·m^{-2}·d^{-1}) was determined by sedimentation rates (S_a, cm·yr^{-1}), sedimentary TOC concentrations (C_{sed}; mg·C·kg^{-1}) and dry sediment density (ρ_s= 2.65 × 10^3 kg·m^{-3}; Bianchi et al., 2013): (I would suggest not use to equation editor inside text, density above)

$$F_D = S_a \times C_{sed} \times \rho_s \qquad (6)$$

Due to the invariant ^{210}Pb profiles in the well mixed upper layer of these shallow estuaries (20-cm cores from our campaigns, D. Hammond, pers. Comm.), we instead applied average sediment accumulation rates based on measurements in Bronikowski (2004) and Yeager et al. (2006) (Table 1). They had successfully derived sedimentation rates in Lavaca Bay (upper LCE) and NE, respectively. In addition, historical surface sedimentary TOC data were obtained from TCEQ and averaged for dry and wet conditions (Table 1) with slight mismatch due to sampling time inconsistency between TCEQ survey and our study. Thus, averaged sedimentation rates under dry and wet conditions were applied to corresponding upper and lower estuarine systems based on their hydrologic similarities (Table 1).

2.9 Oceanic export (F_{EX})

Due to shallow and windy conditions, the estuarine water was assumed to be well mixed (little stratification was observed during our study period), box-modeling approach was then introduced to estimate the net export to the open ocean. The steady-state net carbon export was calculated based on the Land-Ocean Interactions in the Coastal Zone method (LOICZ; Smith et al., 2005):

$$\left.\begin{aligned} V_R &= -(V_{Rv} + V_{SGD} + V_P - V_E) \\ \tau &= \frac{V}{V_X + |V_R|} \\ F_{Ex} &= V_R \times \overline{C} - V_X \times C_{Ocean} \end{aligned}\right\} \quad (7)$$

V_R ($m^3 \cdot d^{-1}$) is the residual freshwater flow between the system and the adjacent open ocean, V_{Rv} is daily river discharge, V_{SGD} is average SGD (Table 1), V_P and V_E denote precipitation and evaporation volume (see in Section 2.5), V_X is exchanged flow between estuary and adjacent open ocean (negative sign denotes export to the coastal ocean, positive sign denotes net import), V is estuary volume that was derived from averaged depth and surface area, τ is water residence time, $\overline{C}$ is average DIC or TOC concentration in lower estuaries, C_{Ocean} is ocean endmember DIC or TOC value (more details in Table 1).

2.10 Calcification (F_{Ca})

Daily calcification rates were calculated as the difference of salinity-normalized Ca^{2+} (nCa_i^{2+}, $mmol \cdot kg^{-1}$; Friis et al., 2003) between every two consecutive campaigns divided by number of days:

$$\left.\begin{aligned} nCa_i^{2+} &= \frac{(\mathrm{Sal}_{ocean} - \mathrm{Sal}_i) \times Ca_{river}^{2+} + (\mathrm{Sal}_i - \mathrm{Sal}_{river}) \times Ca_{ocean}^{2+}}{\mathrm{Sal}_{ocean} - \mathrm{Sal}_{river}} \\ F_{Ca} &= \frac{nCa_i^{2+} - nCa_{i-1}^{2+}}{d_i - d_{i-1}} \end{aligned}\right\} \quad (8)$$

Sal is salinity, subscript *i* denotes the *i*-th campaign, subscript *river* and *ocean* denote the two endmembers values, respectively (Table 1); positive F_{Ca} indicates calcification and negative indicates carbonate dissolution.

2.11 Lateral exchange (F_L)

Lateral exchange of DIC and TOC are the only unknown terms and were calculated as residuals from Eqs. 1 and 2, respectively.

2.12 Area-weighted annual fluxes

Finally, area-weighted annual fluxes of different carbon budget terms were averaged by the sum of all campaigns:

$$\left.\begin{aligned} \overline{F_i} &= \frac{\overline{F_i^{up}} \times S_{up} + \overline{F_i^{low}} \times S_{low}}{S_{up} + S_{low}} \\ F_x &= \frac{\sum_1^i (\overline{F_i} \times d_i)}{\sum_1^i d_i} \end{aligned}\right\} \quad (9)$$

$\overline{F_i^{up}}$ and $\overline{F_i^{low}}$ (mmol·C·d^{-1}) are arithmetic means of carbon fluxes in upper and lower estuaries from campaign *i*, S_{up} and S_{low} are upper and lower surface areas in individual estuaries, $\overline{F_i}$ (mmol·C·m^{-2}·d^{-1}) is area-weighted average flux in campaign *i*, d_i is the duration (days) between two consecutive sampling campaigns, F_x (mol·C·m^{-2}·yr^{-1}) denotes area-weighted annual flux of carbon budget term *x*.

2.12 Uncertainty

Like all budgetary calculations, uncertainties could be amplified when integrating different processes from both calculations- and measurement-associated errors (Table 2). Despite relatively high-resolution sampling for river end-members (Table S1), uncertainty may have been introduced by averaging riverine DIC and TOC loading under dry and wet conditions. The F_{CO2} calculation would incur the uncertainties due to gas transfer velocity parameterization and spatial coverage from limited sampling stations. In addition, F_{NEM} may carry errors due to the empirical F_{CO2}-F_{NEM} relationship. uncertainty in F_D could be due to varying sediment accumulation rate and sedimentary TOC content. Finally, lateral TOC and DIC exchange were calculated as residual from Eqs. 1&2, so they were subject to the error propagation from other fluxes.

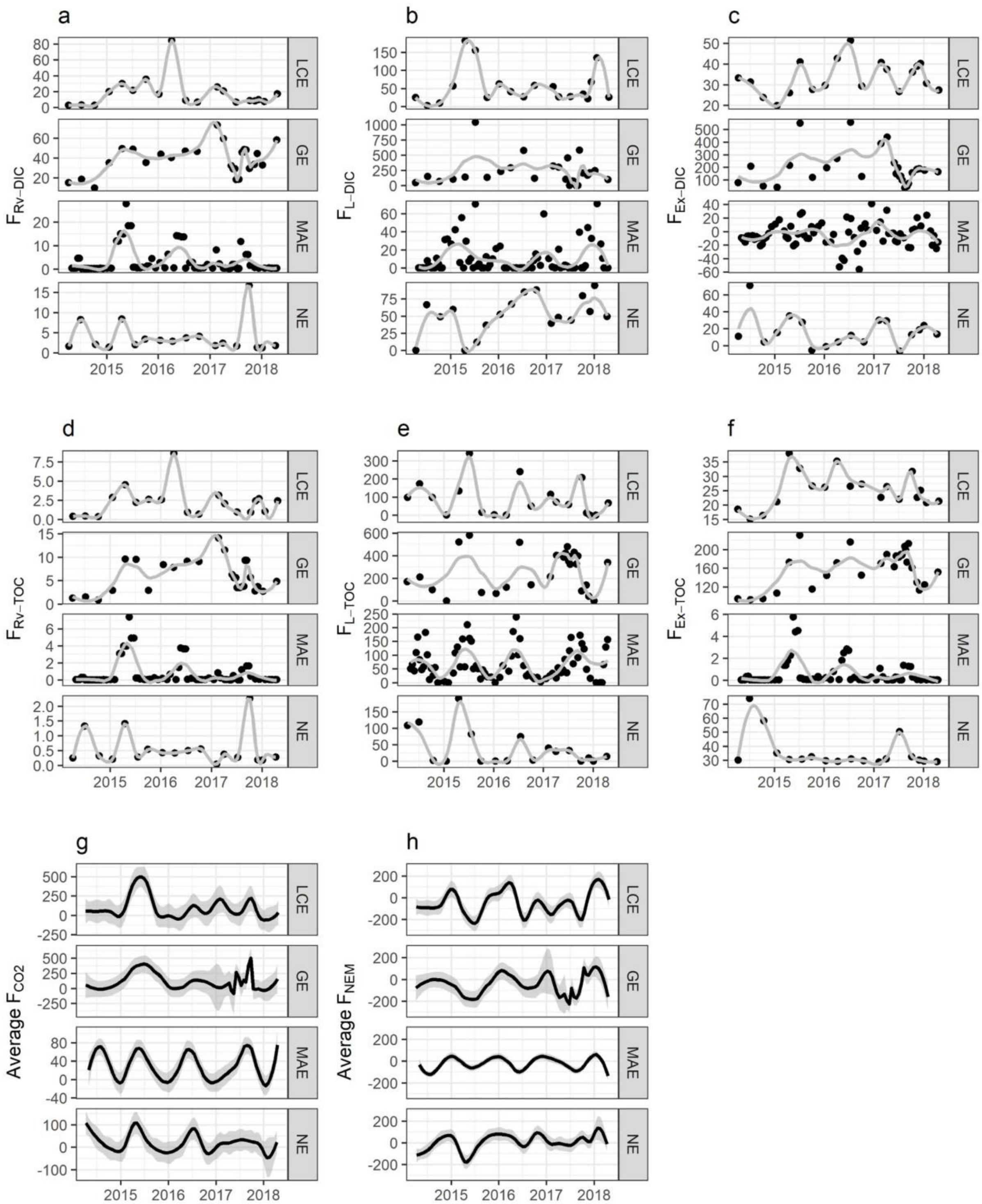

Figure 2. Observed or modeled carbon fluxes in four estuaries. **a**, area-weighted riverine DIC inputs. **b**, area-weighted lateral DIC exchanges. **c**, area-weighted oceanic DIC exports. **d**, area-weighted riverine TOC inputs. **e**, area-weighted lateral TOC exchanges. **f**, area-weighted TOC oceanic exports. **g**, averaged air-water CO_2 flux, shaded areas denote standard deviations. **h**, averaged NEM, shaded areas denote standard deviations. (unit: $mmol{\cdot}C{\cdot}m^{-2}{\cdot}d^{-1}$)

3 Results

3.1 Riverine input

Average river discharge ranged from 107.9 ± 137.8 $m^3 \cdot s^{-1}$ (the uncertainties are all one standard deviations hereafter) in LCE to the north to 8.6 ± 16.9 $m^3 \cdot s^{-1}$ in NE to the south, consistent with the declining trend of inflow from north to south (i.e., LCE to NE, Table 1). Distinct seasonality was observed with high river discharge in spring—summer in response to storm-driven flooding in 2015, 2016 and 2017; but fall—winter had much less discharge. As a result, $F_{Rv\text{-}DIC}$ and $F_{Rv\text{-}TOC}$ had the same seasonal pattern but different magnitudes (Figs. 2a and 2d). During spring—summer flooding period, maximum $F_{Rv\text{-}DIC}$ in LCE and GE reached 84.4 and 59.5 $mmol \cdot C \cdot m^{-2} \cdot d^{-1}$, respectively, while max $F_{Rv\text{-}DIC}$ in MAE and NE were comparably lower (27.8 and 16.7 $mmol \cdot C \cdot m^{-2} \cdot d^{-1}$, respectively) due to smaller river discharges. Similarly, maximum $F_{Rv\text{-}TOC}$ were 8.6 and 14.1 $mmol \cdot C \cdot m^{-2} \cdot d^{-1}$ for LCE and GE, respectively; compared to 7.4 and 2.3 $mmol \cdot C \cdot m^{-2} \cdot d^{-1}$ for MAE and NE, respectively.

3.2 Air-water CO_2 flux

All four estuaries were net CO_2 sources to the atmosphere (Fig. 3) although with distinct spatiotemporal patterns (Fig. 2g). Average F_{CO2} ranged -50 – 500 $mmol \cdot C \cdot m^{-2} \cdot d^{-1}$. In spring and summer, these estuaries had higher CO_2 emission (up to 500 $mmol \cdot C \cdot m^{-2} \cdot d^{-1}$) as a result of flooding (Yao & Hu 2017; Yao et al., 2020). The peak of CO_2 efflux values in LCE and GE (~500 $mmol \cdot C \cdot m^{-2} \cdot d^{-1}$) was fourfold higher than those in MAE and NE (~100 $mmol \cdot C \cdot m^{-2} \cdot d^{-1}$). In comparison, F_{CO2} decreased and even changed sign (-50 – 100 $mmol \cdot C \cdot m^{-2} \cdot d^{-1}$) in fall and winter, when these estuaries became a weak CO_2 sink. Overall, annual average F_{CO2} in LCE and GE was an order of magnitude higher than those in MAE and NE (Fig. 3).

3.3 NEM

The F_{NEM} values were lowest in spring and summer (-45.3 ± 81.5 and -104.0 ± 91.3 mmol·C·m^{-2}·d^{-1}; respectively), indicating an overall heterotrophy. Increasing NEM in fall (-9.4 ± 73.8 mmol·C·m^{-2}·d^{-1}) illustrated weakening heterotrophic activities, and positive NEM in winter (66.4 ± 53.9 mmol·C·m^{-2}·d^{-1}) illustrated autotrophic conditions. Annual F_{NEM} values suggested heterotrophic dominance in northern estuaries (i.e., LCE and GE), whereas MAE was slightly heterotrophically dominant and NE was slightly autotrophically dominant (Fig. 3).

3.4 Sediment deposition

Annual average F_D to sediment was 6.8 ± 2.2 mol·C·m^{-2}·yr^{-1} in LCE, with 13.4 ± 3.7 and 25.3 ± 8.3 mmol·C·m^{-2}·d^{-1} in dry and wet conditions, respectively. F_D was the highest in GE at 14.1 ± 3.2 mol·C·m^{-2}·yr^{-1}, 28.4 ± 3.9 mmol·C·m^{-2}·d^{-1} in dry and 46.7 ± 25.5 mmol·C·m^{-2}·d^{-1} in wet conditions. Then F_D declined toward the south (5.1 ± 5.5 mol·C·m^{-2}·yr^{-1} in MAE and 1.9 ± 0.1 mol·C·m^{-2}·yr^{-1} in NE).

3.5 Export to the coastal ocean

Area-weighted $F_{Ex\text{-}DIC}$ was between -60 – 550 mmol·C·m^{-2}·d^{-1}, and $F_{Ex\text{-}TOC}$ was 0.1 – 230 mmol·C·m^{-2}·d^{-1} in all estuaries combined (Figs. 2c and 2f). The highest monthly $F_{Ex\text{-}DIC}$ and $F_{Ex\text{-}TOC}$ were both found in GE in July 2015, corresponding to the first flood after a long drought during our study period. Occasionally negative $F_{Ex\text{-}DIC}$ in MAE and NE indicated a possible oceanic water supply for these oligotrophic estuaries. Consistent with river inflows, these estuaries exported the most DIC and TOC to the GOM in early summer (62.2 ± 133.8 and 49.6 ± 76.9 mmol·C·m^{-2}·d^{-1}, respectively). Among those peak F_{Ex} values, MAE was found with the lowest F_{Ex} (-3.8 ± 14.5 and 0.8 ± 1.4 mmol·C·m^{-2}·d^{-1} for DIC and TOC, respectively) compared with highest in GE (DIC—250.4 ± 177.0 and TOC—181.5 ± 38.6 mmol·C·m^{-2}·d^{-1}). Minimum

$F_{Ex\text{-}DIC}$ occurred in fall (22.5 ± 50.1 mmol·C·m^{-2}·d^{-1}) and minimum $F_{Ex\text{-}TOC}$ was in spring (30.2 ± 54.2 mmol·C·m^{-2}·d^{-1}), during which minimum $F_{Ex\text{-}DIC}$ ranged from -6.9 ± 16.7 (MAE) to 94.5 ± 53.5 (GE) mmol·C·m^{-2}·d^{-1}, minimum $F_{Ex\text{-}DIC}$ fluctuated between 0.9 ± 1.4 (MAE) and 156.0 ± 36.8 (GE) mmol·C·m^{-2}·d^{-1}.

3.6 Lateral exchange

Although average DIC and DOC fluxes due to SGD in upper NE (~4050 and 840 mmol·C·m^{-2}·d^{-1}, respectively) has been estimated from previous study (Murgulet et al., 2018), these overwhelmingly high carbon inflows are supposed to be balanced by estuarine carbon outflows (Sections 3.2, 3.4 and 3.5). Herein there must be large variations of $F_{L\text{-}DIC}$ and $F_{L\text{-}TOC}$ for each estuary. Due to a possible error amplification from limited data coverage, lateral exchanges were calculated as a residual term from the mass balance model (Eqs. 1 & 2) rather than SGD application.

Area-weighted $F_{L\text{-}DIC}$ ranged from 0 – 1000 mmol·C·m^{-2}·d^{-1}, and $F_{L\text{-}TOC}$ ranged 0 – 580.2 mmol·C·m^{-2}·d^{-1} (Figs. 2b & 2e). GE had the largest annual $F_{L\text{-}DIC}$ and $F_{L\text{-}TOC}$ (Fig. 3) as well as the highest variation. Both $F_{L\text{-}DIC}$ and $F_{L\text{-}TOC}$ peaked in summer, with the maximum estimated in GE during the summer of 2015. In contrast, the four-estuary averaged $F_{L\text{-}DIC}$ reached a minimum (41.3 ± 75.5 mmol·C·m^{-2}·d^{-1}) in spring, while lowest $F_{L\text{-}TOC}$ occurred in winter (21.9 ± 46.1 mmol·C·m^{-2}·d^{-1}).

3.7 Carbon budget

The annual carbon budget in each estuary was calculated by the area-integrated DIC and TOC fluxes (Fig. 3). The largest DIC input was $F_{L\text{-}DIC}$. In particular, $F_{L\text{-}DIC}$ in GE was estimated to be almost sevenfold of $F_{Rv\text{-}DIC}$. On the other hand, F_{CO_2} and $F_{Ex\text{-}DIC}$ were two major DIC loss pathways from nwGOM estuaries. Estuarine CO_2 emission was comparable to DIC export to the ocean. The only exception was GE, where its $F_{Ex\text{-}DIC}$ was twice higher than F_{CO2}. On the organic carbon side, $F_{L\text{-}TOC}$ accounted for approximately 98% of total TOC input, which was almost one order of magnitude higher than $F_{Rv\text{-}TOC}$ in all these estuaries. In LCE and MAE, these TOC inputs roughly equally supported NEM, sediment deposition and oceanic export, whereas oceanic export dominated TOC outflow in GE and NE (69.0% and 88.2% of total TOC input, respectively). On the other hand, compared to F_{Rv}, F_L, F_D, and F_{ex}, F_P and F_{Ca} were small enough to be ignored (Fig. 3).

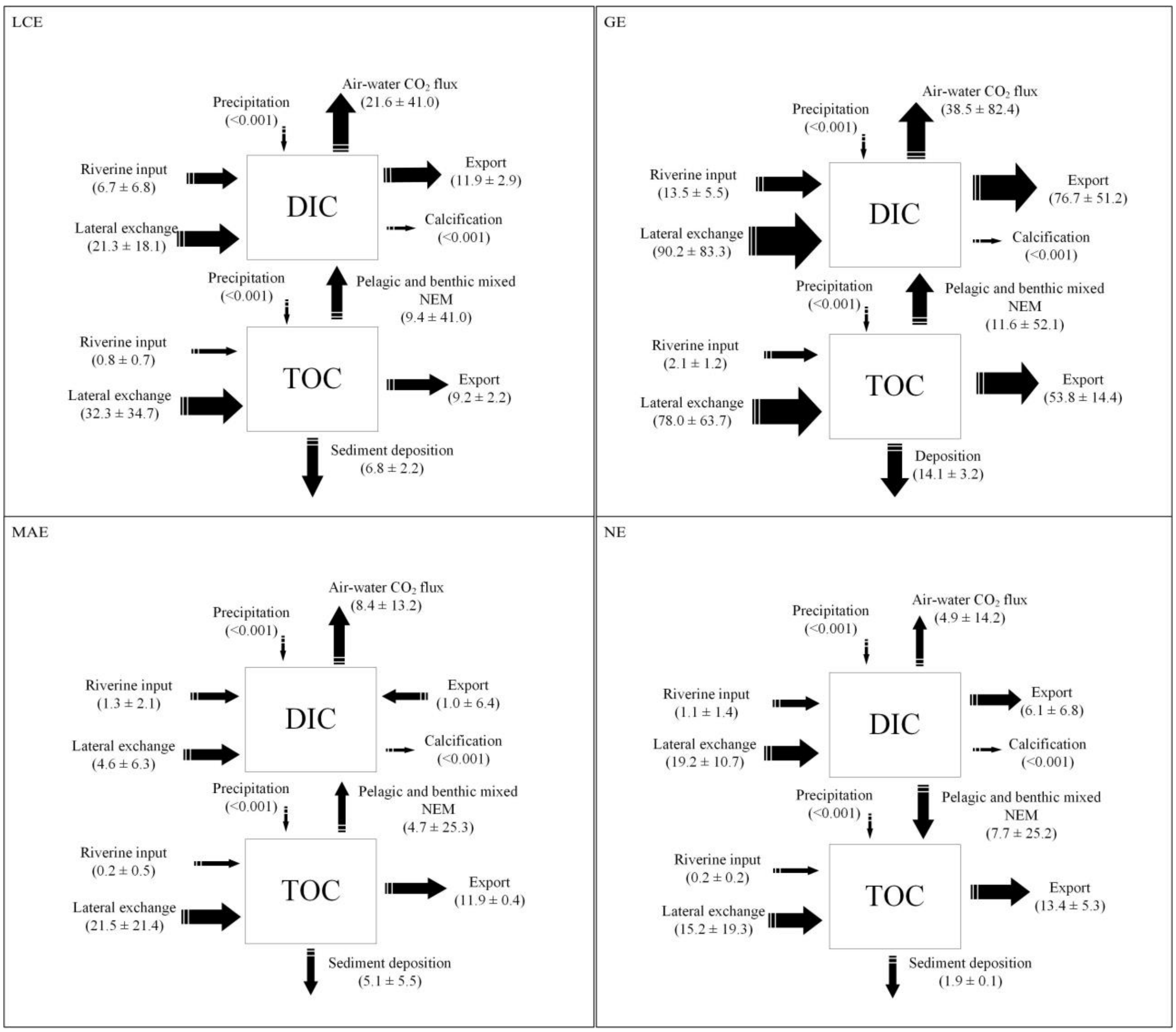

Figure 3. Carbon fluxes for DIC and TOC inventories of four studied estuaries, "±" indicates standard deviation. (unit: $mmol{\cdot}C{\cdot}m^{-2}{\cdot}d^{-1}$)

4 Discussion

4.1 Important lateral exchange from tidal marsh and mangroves

Tidal marsh and mangrove systems are among the most productive ecosystems on earth (Bouillon et al., 2008; Cai, 2011; Hopkinson, 1988). However, their role in the estuarine carbon cycle remains largely unresolved because of difficulties making direct measurements (Bouillon et al., 2008; Sippo et al., 2016; Wang et al., 2016). Nevertheless, lateral carbon exchanges between estuaries and tidal wetlands have been evaluated in previous studies as important to the estuarine carbon budget (Maher et al., 2018; Santos et al., 2019). For example, Maher et al. (2013) found that values for added $\delta^{13}C$-DOC in an estuarine tidal creek (~ -30‰) are similar to mangrove leaves in southern Moreton Bay on the Australian east coast. Wang et al. (2016) also scaled up annual areal DIC export from marshes (34.5 $mol\cdot C\cdot m^{-2}\cdot yr^{-1}$) to the U.S. east coast through direct measurement from tidal exchange. In addition, submarine groundwater was also highlighted for delivering carbon between estuaries and wetlands (Faber et al., 2014; Santos et al., 2019; Douglas et al., 2021).

In this study, annual F_{Rv} only introduced a small portion of total inputs (~ 2.2 % for TOC and ~ 13.7 % for DIC). Given the imbalance between high carbon outflows (CO_2 emission, carbon export and deposition) and relatively small riverine supplies, we predict that lateral exchange must be crucial for carbon budgets in these estuaries despite potentially large uncertainties. The nwGOM coastline has an extensive distribution of saltmarshes and mangroves (Armitage et al., 2015; Saintilan et al., 2009), and mangroves are mostly south of 27˚N, although they are migrating north due to warming (Montagna et al. 2011). By integrating four estuaries, we estimated that $F_{L\text{-}TOC}$ and $F_{L\text{-}DIC}$ were 32.3 ± 4.1 and 27.0 ± 5.3 $mol\cdot C\cdot m^{-2}\cdot yr^{-1}$, respectively. These values are comparable to those of other tidal marsh and mangrove systems (Table 3), suggesting that coastal saltmarshes and mangroves are important carbon sources to nwGOM estuaries. In general, the major mechanisms that drove F_L between saltmarshes/mangroves and estuaries included tidal exchange, groundwater discharge, eddy diffusion, rainstorm, and wind speed and direction (Chalmers et al., 1985; Maher et al., 2018; Maher et al., 2013; Santos et al., 2019; Sippo et al., 2016; Wang et al., 2017; Wang et al., 2016). Tidal exchange was more effective in shallower environments (Sippo et al., 2016). We speculate that the strongest lateral exchange should occur at the top layer of tidal wetland sediments. In fact, Bianchi et al. (2013) pointed out a loss of carbon in the surface layer of mangrove sediment from the lower MAE, based on an unusually low sediment C:N ratio. In addition, Murgulet et al. (2018) observed a strong submarine groundwater discharge, which supplies DIC and total alkalinity in the upper NE area (~ 4.1 and 4.9 $mol \cdot C \cdot m^{-2} \cdot d^{-1}$, respectively). However, given its large spatiotemporal variability (Murgulet et al., 2018; Spalt et al., 2020), more accurate quantification of the lateral exchange would be desired for future estuarine carbon budget studies.

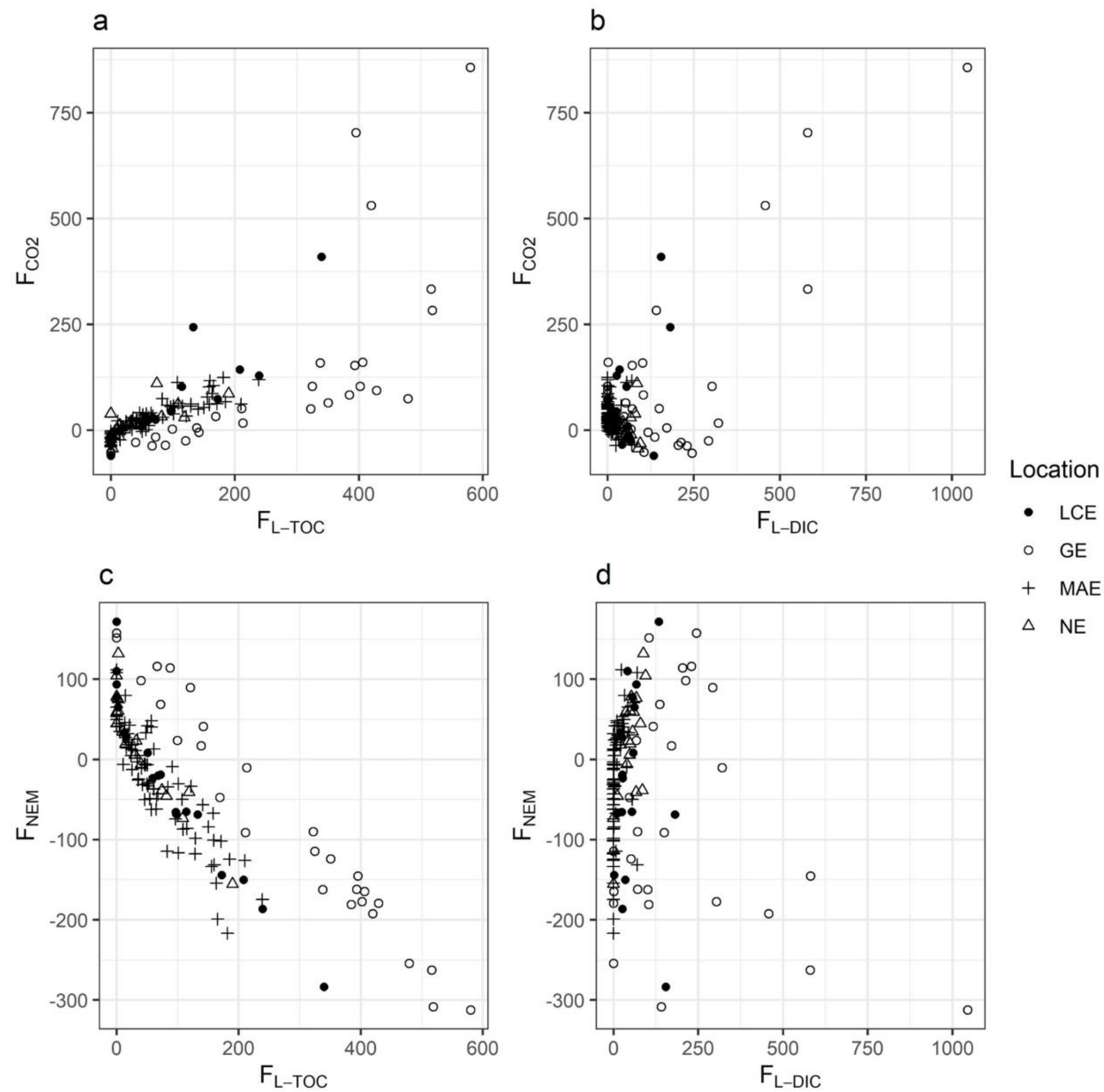

Figure 4. Relationships among different fluxes in four estuaries. **a**, lateral TOC vs. air-water CO_2 flux. **b**, lateral DIC vs. air-water CO_2 flux. **c**, lateral TOC vs. NEM. **d**, lateral DIC vs. NEM. (unit: $mmol \cdot C \cdot m^{-2} \cdot d^{-1}$)

The large imbalance between observed riverine carbon input and estuarine export as well CO_2 efflux highlighted the significance of lateral carbon exchanges. Estuarine F_{CO2} might be largely dependent on F_L (r = 0.734, N = 140 and r = 0.712, N = 140 for TOC and DIC respectively, $p < 0.001$ for both cases; Figs. 4a & b). While $F_{L\text{-}TOC}$ contribute significantly on F_{CO2}

change (Fig. 4a), the effect of $F_{L\text{-}DIC}$ on F_{CO2} varies depending on the estuarine system (seen as inverse correlations between $F_{L\text{-}DIC}$ and F_{CO2} for LCE/GE and MAE/NE, respectively; Fig. 4b). This was presumably attributed to varying primary production rates in different estuaries. For example, lateral DIC seemed to become more important for autotrophic activities in MAE (r = 0.425, p < 0.001, N = 75; Fig. 4d) and NE (r = 0.699, p = 0.001, N = 17; Fig. 4d) as river input dwindles to the south. There increasing $F_{L\text{-}DIC}$ were associated with stronger autotrophic activities (increasing NEM, Fig. 3), which was indicative of declining CO_2 emission or even atmospheric CO_2 uptake. Nevertheless, relatively small $F_{Rv\text{-}TOC}$ (Fig. 3) and relationship between $F_{L\text{-}TOC}$ and F_{NEM} (r = 0.840, N = 140, p < 0.001; Fig. 4c) across four estuaries highlighted the significant support of tidal wetland on estuarine NEM.

Consistent with other studies (Chalmers et al., 1985; Wang et al., 2017; Wang & Cai, 2004; Wang et al., 2016), $F_{L\text{-}TOC}$ and $F_{L\text{-}DIC}$ in nwGOM estuaries had large seasonal variabilities (Figs. 2b & 2e), i.e. high $F_{L\text{-}TOC}$ but low $F_{L\text{-}DIC}$ in April—August while low $F_{L\text{-}TOC}$ but high $F_{L\text{-}DIC}$ in December—February. One explanation is a high DIC uptake due to the maximum growth rate in spring—summer for wetland system (Wang et al., 2017; Wang & Cai, 2004). Additionally, spring—summer floods flushed more surface organic carbon from wetland to estuary (Chalmers et al., 1985). Whereas high DIC:DOC ratio SGD in winter—spring favored the $F_{L\text{-}DIC}$ (Murgulet et al., 2018). Such high winter $F_{L\text{-}DIC}$ might support extensive autotrophy in these estuaries according to concurrent positive NEM and CO_2 uptake (Russell & Montagna, 2007; Yao et al. 2020).

4.2 Hydrologic control on estuarine carbon budget

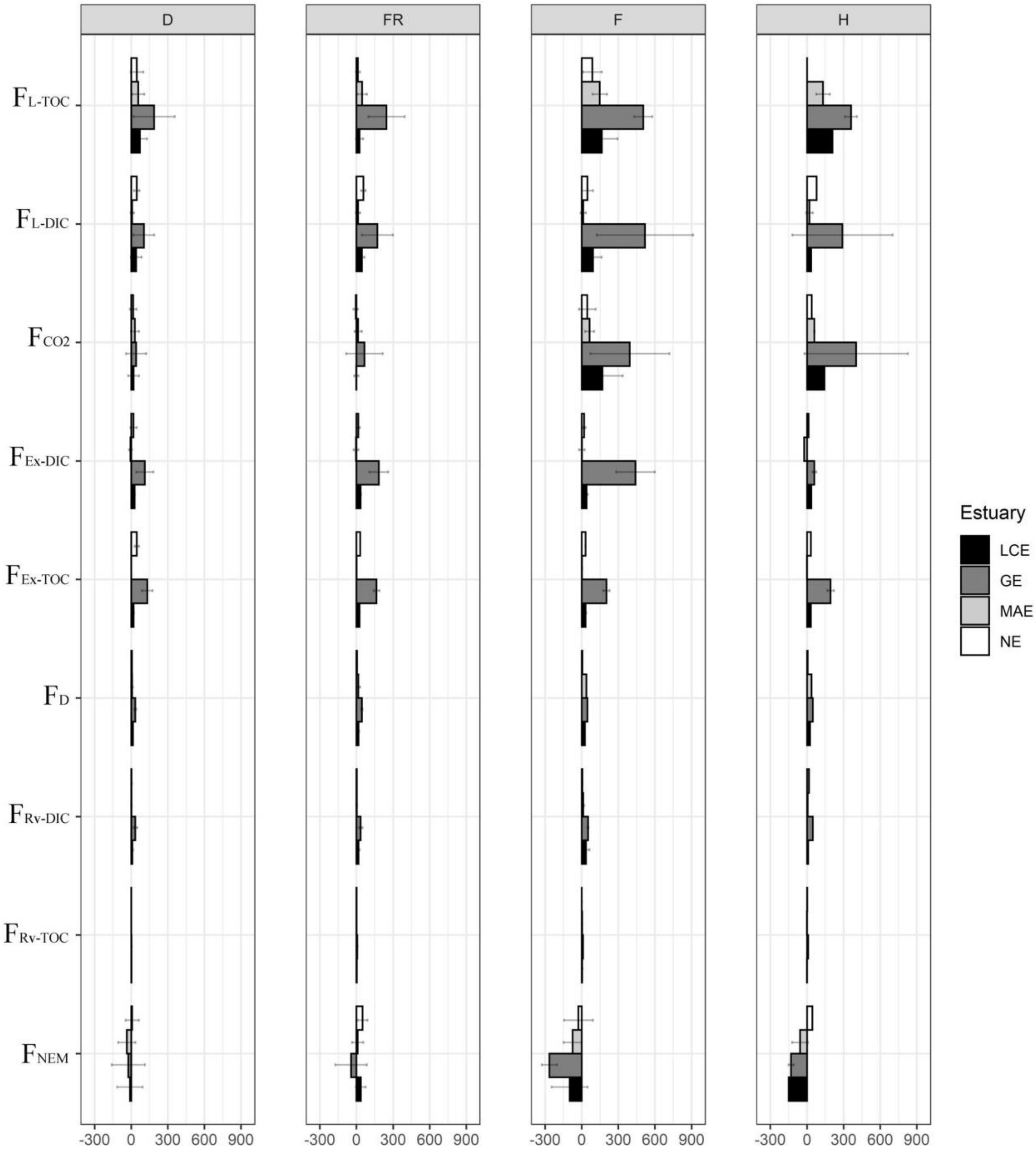

Figure 5. Carbon fluxes under different hydrologic conditions. The headings represent D = drought; FR = flood relaxation; F = flooding; H = hurricane. (unit: $mmol \cdot C \cdot m^{-2} \cdot d^{-1}$)

During our study period, south Texas experienced extreme hydrologic changes from a dry (prior to April 2015) to a wet condition, including a Category 4 hurricane (Hurricane Harvey) influence in fall 2017 (Walker et al., 2020). To further assess the estuarine carbon budget variability under this wide range of hydrologic condition, we assigned two sub-periods under dry and wet conditions by following Palmer and Montagna (2015), respectively: drought and flood relaxation under dry conditions, and flooding and hurricane under wet conditions (hydrologic definitions are based on the quartiles of mean salinities, except for hurricane; Table 4). Both flooding and flood relaxation occurred at multiple periods over time. F_L, F_{CO2} and F_{Ex} experienced the largest changes across different periods (Fig. 5). F_{CO2} indicated strong estuarine CO_2 emission ($22.2 \pm 81.0 – 184.7 \pm 256.6$ mmol·C·m^{-2}·d^{-1}) overall. Flood from Hurricane Harvey increased F_{CO2} by 2 – 10 times compared to baseline values, with the most pronounced increase in LCE (18.90 ± 45.3 to 169.8 ± 166.5 mmol·C·m^{-2}·d^{-1}) and GE (40.1 ± 83.2 to 403.0 ± 424.1 mmol·C·m^{-2}·d^{-1}) compared to MAE (30.6 ± 33.2 to 64.2 ± 38.7 mmol·C·m^{-2}·d^{-1}) and NE (15.6 ± 27.9 to 45.8 ± 68.3 mmol·C·m^{-2}·d^{-1}). Two estuaries, MAE and NE, were on the "dry" side of the storm and riverine input did not substantially increase as shown by their lower area-normalized $F_{Rv\text{-}DIC}$ and $F_{Rv\text{-}TOC}$ (Figs. 2a & 2d). This CO_2 flux increase in LCE and GE was consistent with other similar studies that also found 5 – 10 times elevation of estuarine CO_2 fluxes due to storms or storm-induced flooding (Crosswell et al., 2014; Sarma et al., 2012; Van Dam et al., 2018; Hu et al., 2020). Such increase could be attributed to enhanced post storm remineralization in response to hydrologic condition change as well as riverine CO_2 ventilation (Yao et al. 2020). Walker et al. (2020) also found a strong signature of anoxic riverine water discharge to GE after Hurricane Harvey in 2017. Similarly, $F_{Ex\text{-}DIC}$ and $F_{Ex\text{-}TOC}$ followed the F_{CO2} pattern (Fig. 5). The only exception was the lowest $F_{Ex\text{-}DIC}$ (21.3 ± 35.8 mmol·C·m^{-2}·d^{-1}) during Hurricane Harvey (Fig. 5H), suggesting that CO_2 emission was the major carbon loss term for estuarine system following this extreme yet short-lived disturbance.

Our study assessed the hydrologic effect on lateral exchange of the carbon cycle in nwGOM estuaries. As expected, storm- and hurricane-driven flooding increased $F_{L\text{-}TOC}$ from 90.7 ± 65.7 mmol·C·m^{-2}·d^{-1} (drought) to 200.5 ± 160.2 mmol·C·m^{-2}·d^{-1} (flooding) (Figs. 5D to 5F), and $F_{L\text{-}DIC}$ from 49.1 ± 39.8 mmol·C·m^{-2}·d^{-1} (drought) to 166.9 ± 236.1 mmol·C·m^{-2}·d^{-1} (flooding) (Figs. 5D to 5F). We suspect that these exchanges were most likely caused by large surface runoff (Walker et al., 2020), as submarine groundwater discharge might decrease in their relative significance during flooding (Murgulet et al., 2018). This further confirmed the crucial role of lateral exchange on the carbon budget. Because residence time is a key control on estuarine organic carbon degradation (Hopkinson et al., 1998), the long residence time in these four estuaries (39 – 360 d, Table 1), particularly in MAE and NE, is presumably responsible for such organic carbon processing, hence related carbon fluxes.

Russell et al. (2006) concluded that heterotrophic NEM in this region would not exceed -5 mg·O_2·l^{-1}·d^{-1} (or -312.5 mmol·C·m^{-2}·d^{-1} based on the average depth from Table 1) by integrating open-water and benthic chamber results. Despite the substantial TOC input (33.0 ± 4.1 mmol·C·m^{-2}·d^{-1}), annually aggregated NEM indicates a slight heterotrophy (-4.4 ± 2.2 mol·C·m^{-2}·yr^{-1}) coastwide. The nearly balanced NEM was comparable to other lagoonal estuaries. For example, New River Estuary in North Carolina has NEM between -3.0 – 1.1 mol·C·m^{-2}·yr^{-1} (Crosswell et al., 2017), however its annual F_{CO2} (-0.2 – 2.0 mol·C·m^{-2}·yr^{-1}) was only one tenth of this study. Substantially higher CO_2 flux found in the present study could be attributed to riverine CO_2 ventilation, (e.g. an excess of CO_2 efflux from the river-dominated LCE and GE during extreme flooding; Yao et al. 2020) and the windy conditions year-round (Yao & Hu, 2017). The latter would stimulate gas exchange and CO_2 efflux. For example, the coastwide mean F_{CO2} was 439.3 ± 415.3 mmol·C·m^{-2}·d^{-1} during extreme flooding. Compared to the annual mean value

(46.0 ± 8.3 mmol·C·m^{-2}·d^{-1}), the large increase in CO_2 efflux under flooding conditions indicated that ventilation of river-borne CO_2 accounted for more CO_2 flux than respiration produced CO_2. Nevertheless, the NEM still displayed a range between -312.5 – 283.1 mmol·C·m^{-2}·d^{-1}. Because previous measurements estimated open water NEM to be -250 – 187.5 mmol·C·m^{-2}·d^{-1} during the 2004 flooding season (Russell & Montagna, 2007), the difference from our estimates suggests that approximately 20 – 40% benthic contribution to the overall NEM. Indeed, high sediment oxygen demand is common in these warm subtropical estuaries (Twilley et al., 1999). For example, model simulation in adjacent Galveston Bay illustrated that oxygen concentration could quickly decrease to zero in one hour without benthic photosynthesis (An & Joye, 2001); McCutcheon et al. (2019) also estimated that benthic respiration in Corpus Christi Bay could cause hypoxia within 3 – 25 hours in stratified bottom water.

4.3 Integrated carbon budget and future climate influence

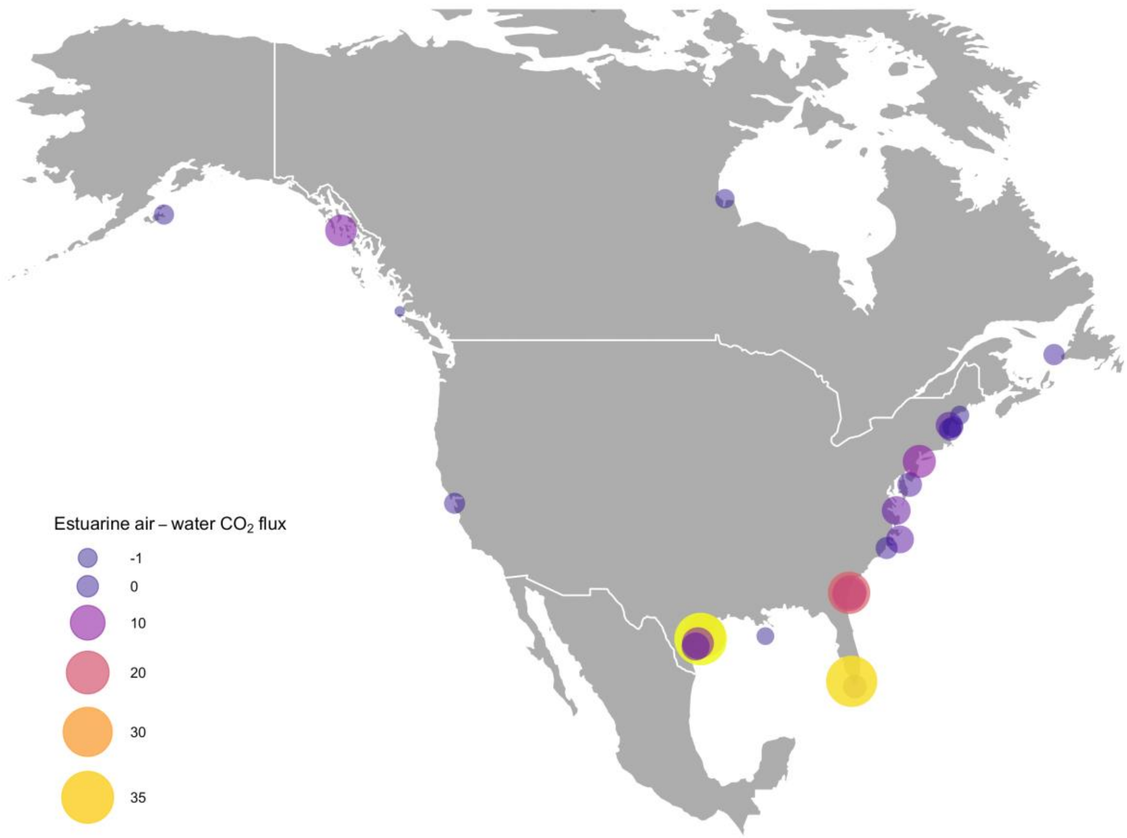

Figure 6. Observed estuarine air-water CO_2 fluxes in North America's coast. (unit: $mol{\cdot}C{\cdot}m^{-2}{\cdot}yr^{-1}$, see details in Table **S2**)

Global estuarine CO_2 emission largely offsets continental shelf CO_2 uptake despite the much smaller area of estuaries (Bauer et al., 2013; Cai, 2011). The annual estuarine CO_2 emission of the nwGOM coast was 16.8 ± 3.0 mol·C·m^{-2}·yr^{-1}, which was more than 3—7 times of the area-weighted average CO_2 emission from North American estuaries (4.6 ± 1.9 mol·C·m^{-2}·yr^{-1} across the Atlantic coast, Najjar et al., 2018; ~2.2 mol·C·m^{-2}·yr^{-1} across the whole North America coast, Chen et al., 2013, Windham-Myers et al., 2018). This was somewhat inconsistent with the values in Windham-Myers et al. (2018), who found GOM estuarine CO_2 flux to be moderate (~8.1 mol·C·m^{-2}·yr^{-1}) among North American coasts. However, syntheses in this study was based on direct observations and recent literature, whereas Windham-Myers et al. (2018) results were partially based on simulations (there were only two observations for GOM estuarine CO_2 flux: Florida Bay 3.93 ± 0.91 mol·C·m^{-2}·yr^{-1} from Zhang and Fischer, 2014; MAE 12.4 ± 3.3 mol·C·m^{-2}·yr^{-1} from Yao and Hu, 2017). Nevertheless, given that previous syntheses were heavily skewed towards Atlantic Coast estuaries and reported relatively low CO_2 emissions in North American estuaries (Chen et al., 2013; Najjar et al., 2018), our findings highlight the diverse set of responses that can be expected in different estuaries and the current lack of spatial coverage in estuarine flux studies (Fig. 6). In addition, revised F_{CO2} from the North American coast could be as much as 7.5 ± 10.9 mol·C·m^{-2}·yr^{-1} if current GOM estuarine records were included (Table 5).

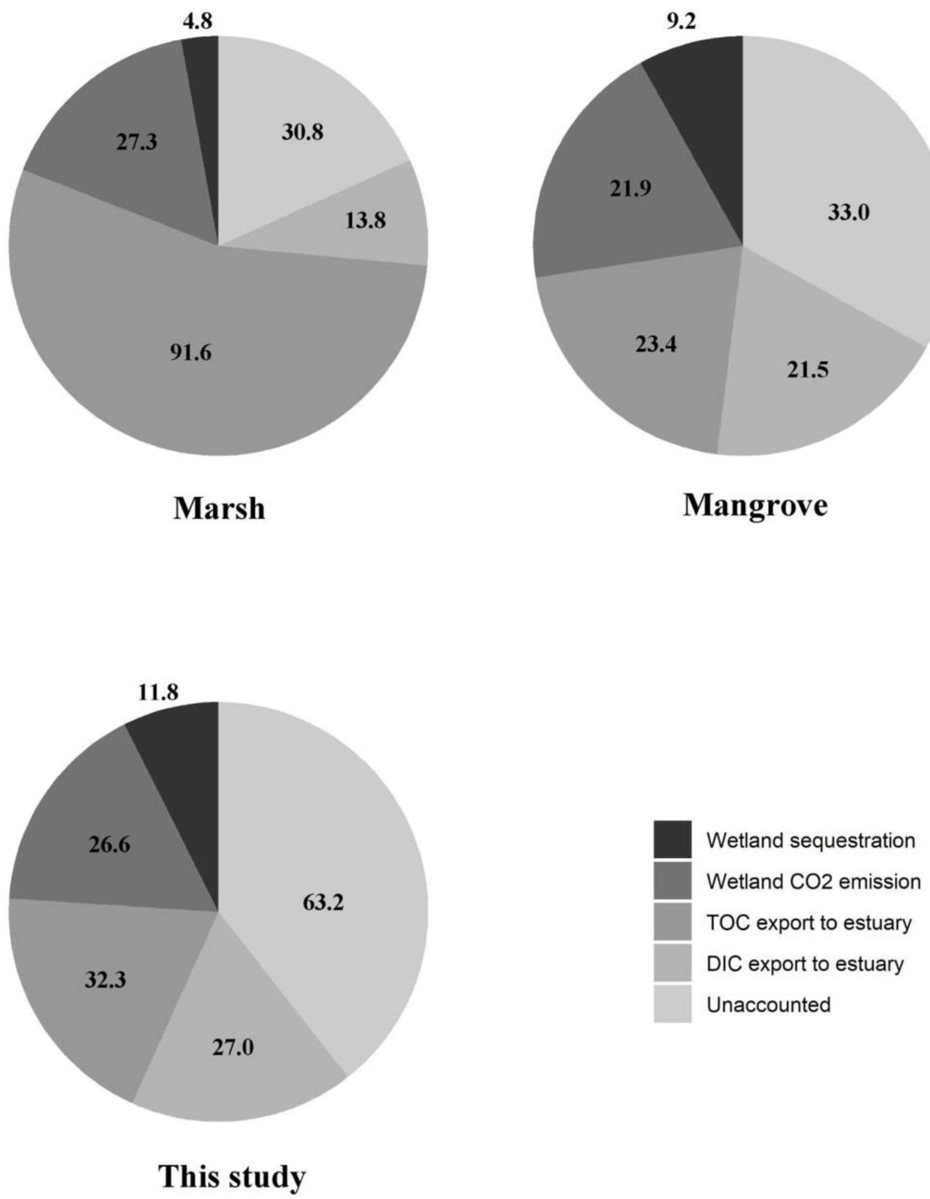

Figure 7. Comparison of area-weighted carbon fluxes between saltmarsh, mangrove, and mixed type. In which marsh data are from Cai (2011) on Southern Atlantic Coast evaluation; mangrove data are from Bouillon et al. (2008) and Sippo et al. (2016) on global evaluation; mixed type data are from this study on nwGOM Coast evaluation. For this study, lateral TOC and DIC (export to estuary) are estimated by mass balance model, wetland sequestration is proportionally from direct measurements in MAE (Bianchi et al., 2013), total fixed carbon and wetland CO_2 emission are integrated values from literatures (Cai 2011; Bouillon et al., 2008; Sippo et al., 2016) (unit: $mol{\cdot}C{\cdot}m^{-2}{\cdot}yr^{-1}$)

Based on the current study and existing literature, the higher estuarine CO_2 emissions are mostly in shallow (< 5 m) subtropical regions surrounded by extensive tidal wetlands (nwGOM, Florida Coast, Southern Atlantic Coast, Fig. 6; Table S2). One important reason for the high CO_2 flux was due to high riverine CO_2 in the southern U.S. (pCO_2 ranged 4000 – 6000 μatm; Butman & Raymond, 2011) or high year-round wind speeds (Yao and Hu, 2017). In comparison, lateral carbon exchange from saltmarshes and mangroves have not been adequately accounted for in explaining estuarine CO_2 flux. The ratio of marsh to mangrove is about 6.4:1 along the nwGOM coastline, an area 240.4×10^3 and 37.9×10^3 km^2 respectively along the entire Texas coast (Armitage et al., 2015). We applied this ratio to estimate regional total carbon fixation and wetland CO_2 ventilation based on previous studies (Fig. 7). Specifically, we assumed total carbon fixation in this area was ~ 160.3 $mol \cdot C \cdot m^{-2} \cdot yr^{-1}$, based on the 6.4:1 ratio of saltmarsh production rate to mangrove production rate (saltmarsh was 168.3 $mol \cdot C \cdot m^{-2} \cdot yr^{-1}$ from the Southern Atlantic Coast, Cai 2011; mangrove production rate was 109 $mol \cdot C \cdot m^{-2} \cdot yr^{-1}$ from global estimates, Bouillon et al., 2008). If assuming wetland carbon sequestration (11.8 $mol \cdot C \cdot m^{-2} \cdot yr^{-1}$, Fig. 7) was about threefold higher than the global average 4.8 $mol \cdot C \cdot m^{-2} \cdot yr^{-1}$ (Chmura et al., 2003), together with estimated estuarine carbon deposition rate 6.3 ± 0.9 $mol \cdot C \cdot m^{-2} \cdot yr^{-1}$ (this study), nwGOM coast would be an important carbon storage region (also known as the "blue carbon", 18.1 $mol \cdot C \cdot m^{-2} \cdot yr^{-}$). Nevertheless, the large spatiotemporal variability highlights the necessity of improved re-evaluation of coastal carbon deposition, particularly with respect to future estuarine sedimentary carbon flux research to better constrain the rate of blue carbon preservation.

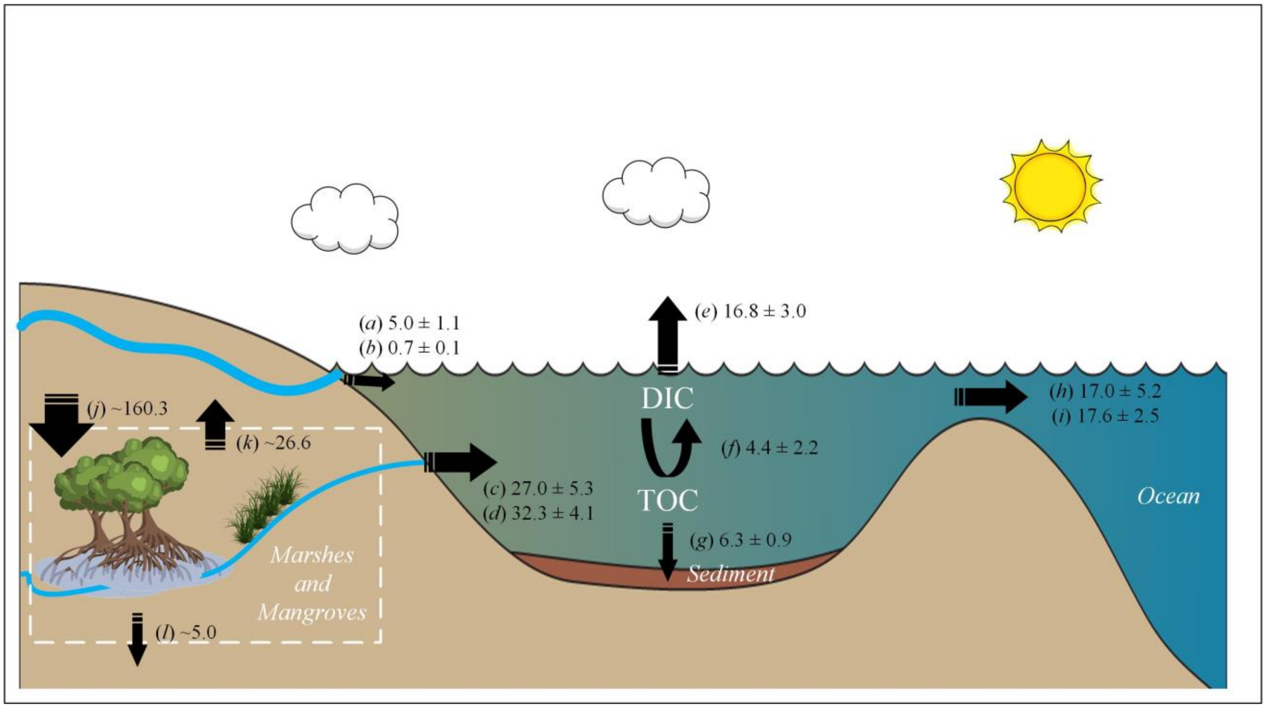

Figure 8. Schematic representation of integrated carbon fluxes in the nwGOM coast. (a) riverine DIC input; (b) riverine TOC input; (c) lateral DIC exchange between tidal wetland and estuary (d) lateral TOC exchange between tidal wetland and estuary; (e) air-water CO_2 flux; (f) pelagic and benthic mixed NEM; (g) sediment TOC deposition; (h) DIC export to open ocean; (i) TOC export to open ocean; (j) carbon fixation by tidal wetland; (k) CO_2 evasion from tidal wetland; (l) carbon sequestration within tidal wetland. (unit: $mol{\cdot}C{\cdot}m^{-2}{\cdot}yr^{-1}$)

Meanwhile, almost 40% of these fixed carbons were estimated export to estuarine water, either via DIC or TOC in this study (Fig. 7). $F_{L\text{-}DIC}$ and $F_{L\text{-}TOC}$ contributed 74.2% and 97.9% of DIC and TOC inputs to nwGOM estuaries, respectively (Fig. 8). With riverine input alone it would be impossible to sustain such high carbon outflows without lateral exchange from tidal wetlands—approximately half of the lateral DIC was to support CO_2 emission and the other half for oceanic export; 15.5% of lateral TOC was remineralized, 22.3% was deposited and the remaining 62.2% was exported to the coastal ocean. Therefore, biogeochemistry in nwGOM estuarine systems appears to largely depend on its extended tidal wetlands (Figs. 3 & 8).

The nwGOM coast had recorded 77.8×10^3 km^2 of total saltmarsh loss from 1990 to 2010, which was a 24% net decrease under the influences of sea level rise and climate change (Armitage et al., 2015). Despite the northward mangrove expansion of 16.1×10^3 km^2 between 1990 and 2010 (Armitage et al., 2015), there was an overall 61.7 km^2 yr^{-1} (~ 1% per year) net loss of marsh-mangrove area in the last two decades. Consequently, we estimated ~ 0.2 and ~ 0.1 $mol \cdot C \cdot m^{-2} \cdot yr^{-1}$ decline of $F_{L\text{-}TOC}$ and $F_{L\text{-}DIC}$ respectively, amounting up to 0.6% and 0.3% of total annual TOC and DIC inputs from combined F_{Rv} and F_L. This decline can be translated to approximate declines of 0.4% F_{CO2}, 0.4% $F_{Ex\text{-}DIC}$, 0.7% $F_{Ex\text{-}TOC}$ and 0.8% F_D (or 0.07, 0.07, 0.12, 0.05 $mol \cdot C \cdot m^{-2} \cdot yr^{-1}$, respectively). In contrast to floods that promoted estuarine carbon fluxes (Fig. 5), sea level rise would decrease estuarine CO_2 flux by submerging tidal wetlands with intruding open ocean waters. Thus, global climate change would alter estuarine carbon fluxes differently, which highlights the necessity of long-term regional focus to predict the future coastal carbon budget trajectories.

5 Conclusions

The coastal carbon budget is important and highly dynamic. Our mass balance model indicated that lateral exchange from saltmarsh and mangrove habitats as a key driver to subtropical nwGOM lagoonal estuaries. For example, lateral TOC exchange could exceed riverine TOC input more than ten times, accounting for almost 97.9% of total TOC input to the estuary. Given the extensive distribution of marsh-mangrove ecotones in the nwGOM coast, more data on lateral carbon exchange is needed to improve accuracy in future forecasts. Due to tidal wetland carbon supply, the entire region served as an important CO_2 source to the atmosphere and also preserved a considerable amount of blue carbon. In addition, the unforeseen high estuarine air-water CO_2 fluxes demonstrated the need for expanding studies focused on carbon cycling along the GOM coast to better constrain the North American coastal carbon budget.

Attempts to assess coastal carbon budget variability requires incorporation of estuarine hydrology. Our four-year dataset over various hydrologic conditions revealed as much as 2 – 10 times increase in estuarine CO_2 flux driven by floods compared with non-flooding (or dry) periods. However, the magnitude of change depended on estuarine residence time and the amount of freshwater inflow that each estuary received. Other than hydrology, nwGOM tidal wetland losses may cause a decline in estuarine carbon fluxes over time. In this study, it was estimated that 0.9% and 0.6% per year declines of TOC and DIC inputs in conjunction with net saltmarsh loss would occur. Nevertheless, a better spatiotemporal carbon budget interpretation, that integrates the estuarine and tidal wetland system, is necessary for future estuarine research under the context of climate change on the coastal and, ultimately, global carbon cycles.

Acknowledgements

We are grateful for the fieldwork assistance provided by the staff and students at both the Mission Aransas National Estuarine Research Reserve and Harte Research Institute at Texas A&M University-Corpus Christi. This study was funded by NOAA's NOS National Center for Coastal Ocean Science (Contract No. NA15NOS4780185) and NSF Chemical Oceanography Program (OCE #1654232, OCE#1760006). This research was also supported in part by operations grants to the Mission-Aransas National Estuarine Research Reserve from NOAA's Office of Coastal Management. The supporting data archiving is underway, it can be found later in public data repository of NOAA National Centers for Environmental Information (NCEI), https://www.bco-dmo.org/dataset/784673.

Reference

An, S., & Joye, S. B. (2001). Enhancement of coupled nitrification - denitrification by benthic photosynthesis in shallow estuarine sediments. *Limnology and Oceanography, 46*(1), 62-74.

Armitage, A. R., Highfield, W. E., Brody, S. D., & Louchouarn, P. (2015). The contribution of mangrove expansion to salt marsh loss on the Texas Gulf Coast. *PLoS One, 10*(5), e0125404. https://doi.org/10.1371/journal.pone.0125404

Bauer, J. E., Cai, W. J., Raymond, P. A., Bianchi, T. S., Hopkinson, C. S., & Regnier, P. A. (2013). The changing carbon cycle of the coastal ocean. *Nature, 504*(7478), 61-70. http://www.ncbi.nlm.nih.gov/pubmed/24305149

Benway, H., & Coble, P. (2014). Report of The US Gulf of Mexico Carbon Cycle Synthesis Workshop, March 27-28, 2013. *Ocean Carbon and Biogeochemistry Program and North American Carbon Program*.

Bianchi, T. S., Allison, M. A., Zhao, J., Li, X., Comeaux, R. S., Feagin, R. A., & Kulawardhana, R. W. (2013). Historical reconstruction of mangrove expansion in the Gulf of Mexico: linking climate change with carbon sequestration in coastal wetlands. *Estuarine, Coastal and Shelf Science, 119*, 7-16.

Bianchi, T. S., Pennock, J. R., & Twilley, R. R. (1999). *Biogeochemistry of Gulf of Mexico estuaries*: John Wiley & Sons.

Borges, A. V., Delille, B., & Frankignoulle, M. (2005). Budgeting sinks and sources of CO_2 in the coastal ocean: Diversity of ecosystems counts. *Geophysical Research Letters, 32*(14).

Borges, A. V., Schiettecatte, L. S., Abril, G., Delille, B., & Gazeau, F. (2006). Carbon dioxide in European coastal waters. *Estuarine, Coastal and Shelf Science, 70*(3), 375-387.

Bouillon, S., Borges, A. V., Castañeda - Moya, E., Diele, K., Dittmar, T., Duke, N. C., et al. (2008). Mangrove production and carbon sinks: a revision of global budget estimates. *Global Biogeochemical Cycles, 22*(2).

Bronikowski, J. L. (2004). *Sedimentary environments and processes in a shallow, Gulf Coast Estuary-Lavaca Bay, Texas.* Texas A&M University,

Butman, D., & Raymond, P. A. (2011). Significant efflux of carbon dioxide from streams and rivers in the United States. *Nature Geoscience, 4*(12), 839-842.

Cai, W. J. (2011). Estuarine and coastal ocean carbon paradox: CO_2 sinks or sites of terrestrial carbon incineration? *Ann Rev Mar Sci, 3*, 123-145. http://www.ncbi.nlm.nih.gov/pubmed/21329201

Carter, B. R., Radich, J. A., Doyle, H. L., & Dickson, A. G. (2013). An automated system for spectrophotometric seawater pH measurements. *Limnology and Oceanography: Methods, 11*, 16-27.

Chalmers, A. G., Wiegert, R. G., & Wolf, P. L. (1985). Carbon balance in a salt marsh: Interactions of diffusive export, tidal deposition and rainfall-caused erosion. *Estuarine, Coastal and Shelf Science, 21*(6), 757-771. http://www.sciencedirect.com/science/article/pii/027277148590071X

Chen, C. T. A., Huang, T. H., Chen, Y. C., Bai, Y., He, X., & Kang, Y. (2013). Air–sea exchanges of CO_2 in the world's coastal seas. *Biogeosciences, 10*(10), 6509-6544.

Chmura, G. L., Anisfeld, S. C., Cahoon, D. R., & Lynch, J. C. (2003). Global carbon sequestration in tidal, saline wetland soils. *Global Biogeochemical Cycles, 17*(4).

Crosswell, J. R., Anderson, I. C., Stanhope, J. W., Van Dam, B., Brush, M. J., Ensign, S., et al. (2017). Carbon budget of a shallow, lagoonal estuary: Transformations and source-sink dynamics along the river-estuary-ocean continuum. *Limnology and Oceanography, 62,* S29-S45.

Crosswell, J. R., Wetz, M. S., Hales, B., & Paerl, H. W. (2014). Extensive CO_2 emissions from shallow coastal waters during passage of Hurricane Irene (August 2011) over the Mid-Atlantic coast of the U.S.A. *Limnology and Oceanography, 59*(5), 1651-1665.

Dickson, A. G. (1990). Standard potential of the reaction: AgCl(s)+ $12H_2$(g)= Ag(s)+ HCl(aq), and and the standard acidity constant of the ion HSO_4^- in synthetic sea water from 273.15 to 318.15 K. *The Journal of Chemical Thermodynamics, 22*(2), 113-127.

Dickson, A. G., J. D. Afghan, & Anderson, G. C. (2003). Reference materials for oceanic CO2 analysis: a method for the certification of total alkalinity. *Marine Chemistry,* 80(2), 185-197. doi:10.1016/S0304-4203(02)00133-0

Douglas, A. R., Murgulet, D., & Montagna, P. A. (2021). Hydroclimatic variability drives submarine groundwater discharge and nutrient fluxes in an anthropogenically disturbed, semi-arid estuary. *Science of The Total Environment*, 142574. https://doi.org/10.1016/j.scitotenv.2020.142574

Douglas, A. R., Murgulet, D., & Peterson, R. N. (2020). Submarine groundwater discharge in an anthropogenically disturbed, semi-arid estuary. *Journal of Hydrology*, 580, 124369. doi:https://doi.org/10.1016/j.jhydrol.2019.124369

Dürr, H. H., Laruelle, G. G., van Kempen, C. M., Slomp, C. P., Meybeck, M., & Middelkoop, H. (2011). Worldwide typology of nearshore coastal systems: Defining the estuarine filter of river inputs to the oceans. *Estuaries and Coasts, 34*(3), 441-458.

Faber, P. A., Evrard, V., Woodland, R. J., Cartwright, I. C., & Cook, P. L. M. (2014). Pore-water exchange driven by tidal pumping causes alkalinity export in two intertidal inlets.

Limnology and Oceanography, 59(5), 1749-1763. https://aslopubs.onlinelibrary.wiley.com/doi/abs/10.4319/lo.2014.59.5.1749

Friis, K., Körtzinger, A., & Wallace, D. W. R. (2003). The salinity normalization of marine inorganic carbon chemistry data. *Geophysical Research Letters, 30*(2). https://agupubs.onlinelibrary.wiley.com/doi/abs/10.1029/2002GL015898

Gordon, D., Boudreau, P., Mann, K., Ong, J., Silvert, W., Smith, S., et al. (1996). *LOICZ biogeochemical modelling guidelines* (Vol. 5): LOICZ Core Project, Netherlands Institute for Sea Research Yerseke.

Herrmann, M., Najjar, R. G., Kemp, W. M., Alexander, R. B., Boyer, E. W., Cai, W.-J., . . . Smith, R. A. (2015). Net ecosystem production and organic carbon balance of U.S. East Coast estuaries: A synthesis approach. *Global Biogeochemical Cycles*, 29(1), 96-111. doi:10.1002/2013gb004736

Ho, D. T., Coffineau, N., Hickman, B., Chow, N., Koffman, T., & Schlosser, P. (2016). Influence of current velocity and wind speed on air - water gas exchange in a mangrove estuary. *Geophysical Research Letters, 43*(8), 3813-3821.

Ho, D. T., Ferrón, S., Engel, V. C., Larsen, L. G., & Barr, J. G. (2014). Air-water gas exchange and CO2 flux in a mangrove-dominated estuary. *Geophysical Research Letters, 41*(1), 108-113.

Hopkinson, C. S. (1988). Patterns of organic carbon exchange between coastal ecosystems. In *Coastal-Offshore Ecosystem Interactions* (Vol. 22, pp. 122-154). Berlin, Heidelberg: Springer.

Hopkinson, C. S., Buffam, I., Hobbie, J., Vallino, J., Perdue, M., Eversmeyer, B., et al. (1998). Terrestrial inputs of organic matter to coastal ecosystems: an intercomparison of chemical characteristics and bioavailability. *Biogeochemistry, 43*(3), 211-234.

Hu, X., Yao, H., Staryk, C. J., McCutcheon, M. R., Wetz, M. S., & Walker, L. (2020). Disparate Responses of Carbonate System in Two Adjacent Subtropical Estuaries to the Influence of Hurricane Harvey – A Case Study. *Frontiers in Marine Science*, 7(26). doi:10.3389/fmars.2020.00026

Jiang, L. Q., Cai, W. J., & Wang, Y. (2008). A comparative study of carbon dioxide degassing in river- and marine-dominated estuaries. *Limnology and Oceanography, 53*(6), 2603-2615.

Kanamori, S., & Ikegami, H. (1980). Computer-processed potentiometric titration for the determination of calcium and magnesium in sea water. *Journal of the Oceanographical Society of Japan, 36*(4), 177-184.

Kemp, W., Smith, E., Marvin-DiPasquale, M., & Boynton, W. (1997). Organic carbon balance and net ecosystem metabolism in Chesapeake Bay. *MARINE ECOLOGY PROGRESS SERIES*, 229-248.

Laruelle, G. G., Goossens, N., Arndt, S., Cai, W.-J., & Regnier, P. (2017). Air–water CO2 evasion from US East Coast estuaries. *Biogeosciences, 14*(9), 2441-2468.

Laruelle, G. G., Dürr, H. H., Lauerwald, R., Hartmann, J., Slomp, C. P., Goossens, N., & Regnier, P. A. G. (2013). Global multi-scale segmentation of continental and coastal waters from the watersheds to the continental margins. *Hydrology and Earth System Sciences*, 17(5), 2029-2051. doi:10.5194/hess-17-2029-2013

Maher, D. T., Call, M., Santos, I. R., & Sanders, C. J. (2018). Beyond burial: lateral exchange is a significant atmospheric carbon sink in mangrove forests. *Biology Letters, 14*(7), 20180200. https://royalsocietypublishing.org/doi/abs/10.1098/rsbl.2018.0200

Maher, D. T., & Eyre, B. D. (2012). Carbon budgets for three autotrophic Australian estuaries: Implications for global estimates of the coastal air-water CO2 flux. *Global Biogeochemical Cycles*, *26*(1).

Maher, D. T., Santos, I. R., Golsby-Smith, L., Gleeson, J., & Eyre, B. D. (2013). Groundwater-derived dissolved inorganic and organic carbon exports from a mangrove tidal creek: The missing mangrove carbon sink? *Limnology and Oceanography, 58*(2), 475-488.

McCutcheon, M. R., Staryk, C. J., & Hu, X. (2019). Characteristics of the Carbonate System in a Semiarid Estuary that Experiences Summertime Hypoxia. *Estuaries and Coasts*, 1-15.

Millero, F. J. (2010). Carbonate constants for estuarine waters. *Marine and Freshwater Research, 61*, 139-142.

Montagna, P.A., Brenner, J., Gibeaut, j., & Morehead, S. (2011). Coastal Impacts. In: Schmandt, J., G.R. North, and J. Clarkson (eds.), *The Impact of Global Warming on Texas, second edition*. University of Texas Press, Austin, Texas, pp. 96-123.

Montagna, P., Palmer, T. A., & Pollack, J. (2013). *Hydrological Changes and Estuarine Dynamics*: Springer Briefs in Environmental Sciences, New York, New York. doi:10.1007/978-1-4614-5833-3.

Montagna, P. A., & Kalke, R. D. (1992). The effect of freshwater inflow on meiofaunal and macrofaunal populations in the Guadalupe and Nueces estuaries, Texas. *Estuaries, 15*(3), 307-326.

Murgulet, D., Murgulet, V., Spalt, N., Douglas, A., & Hay, R. G. (2016). Impact of hydrological alterations on river-groundwater exchange and water quality in a semi-arid area: Nueces River, Texas. *Science of the Total Environment, 572*, 595-607.

Murgulet, D., Trevino, M., Douglas, A., Spalt, N., Hu, X., & Murgulet, V. (2018). Temporal and spatial fluctuations of groundwater-derived alkalinity fluxes to a semiarid coastal embayment. *Science of the Total Environment, 630*, 1343-1359.

Najjar, R. G., Herrmann, M., Alexander, R., Boyer, E. W., Burdige, D. J., Butman, D., et al. (2018). Carbon budget of tidal wetlands, estuaries, and shelf waters of eastern North America. *Global Biogeochemical Cycles, 32*(3), 389-416.

Orr, J. C., Epitalon, J.-M., Dickson, A. G., & Gattuso, J.-P. (2018). Routine uncertainty propagation for the marine carbon dioxide system. *Marine Chemistry, 207*, 84-107.

Paerl, H. W., Crosswell, J. R., Van Dam, B., Hall, N. S., Rossignol, K. L., Osburn, C. L., . . . Harding, L. W. (2018). Two decades of tropical cyclone impacts on North Carolina’s estuarine carbon, nutrient and phytoplankton dynamics: implications for biogeochemical cycling and water quality in a stormier world. *Biogeochemistry*, 141(3), 307-332. doi:10.1007/s10533-018-0438-x

Palmer, T. A., & Montagna, P. A. (2015). Impacts of droughts and low flows on estuarine water quality and benthic fauna. Hydrobiologia, 753(1), 111-129. doi:10.1007/s10750-015-2200-x

Regnier, P., Friedlingstein, P., Ciais, P., Mackenzie, F. T., Gruber, N., Janssens, I. A., et al. (2013). Anthropogenic perturbation of the carbon fluxes from land to ocean. *Nature Geoscience, 6*(8), 597–607.

Russell, M. J., & Montagna, P. A. (2007). Spatial and temporal variability and drivers of net ecosystem metabolism in western Gulf of Mexico estuaries. *Estuaries and Coasts, 30*(1), 137-153.

Russell, M. J., Montagna, P. A., & Kalke, R. D. (2006). The effect of freshwater inflow on net ecosystem metabolism in Lavaca Bay, Texas. *Estuarine, Coastal and Shelf Science, 68*(1-2), 231-244.

Saintilan, N., Rogers, K., & McKee, K. (2009). Salt marsh-mangrove interactions in Australasia and the Americas. In *Coastal wetlands an integrated ecosystem approach* (pp. 855-884). Amsterdam; Boston: Elsevier.

Santos, I. R., Maher, D. T., Larkin, R., Webb, J. R., & Sanders, C. J. (2019). Carbon outwelling and outgassing vs. burial in an estuarine tidal creek surrounded by mangrove and saltmarsh wetlands. *Limnology and Oceanography, 64*(3), 996-1013. https://aslopubs.onlinelibrary.wiley.com/doi/abs/10.1002/lno.11090

Sarma, V. V. S. S., Viswanadham, R., Rao, G. D., Prasad, V. R., Kumar, B. S. K., Naidu, S. A., et al. (2012). Carbon dioxide emissions from Indian monsoonal estuaries. *Geophysical Research Letters, 39*(3).

Sippo, J. Z., Maher, D. T., Tait, D. R., Holloway, C., & Santos, I. R. (2016). Are mangroves drivers or buffers of coastal acidification? Insights from alkalinity and dissolved inorganic carbon export estimates across a latitudinal transect. *Global Biogeochemical Cycles, 30*(5), 753-766.

Smith, S., Buddemeier, R., Wulff, F., Swaney, D., Camacho-Ibar, V., David, L., . . . McLaughlin, C. (2005). C, N, P fluxes in the coastal zone. In C.J. Crossland, H.H. Kremer, H.J.

Lindeboom, J.I. Marshall Crossland, & M. D. A. L. Tissier (Eds.), *Coastal Fluxes in the Anthropocene* (pp. 95-143): Springer.

Smith, S. V., Hollibaugh, J. T., Dollar, S. J., & Vink, S. (1991). Tomales Bay Metabolism: C-N-P Stoichiometry and Ecosystem Heterotrophy at the Land-Sea Interface. *Estuarine, Coastal and Shelf Science, 33*(3), 223-257.

Solis, R., & Powell, G. (1999). Hydrography, mixing characteristics, and residence times of Gulf of Mexico estuaries. In *Biogeochemistry of Gulf of Mexico estuaries* (pp. 29-61): John Wiley & Sons.

Spalt, N., Murgulet, D., & Abdulla, H. (2020). Spatial variation and availability of nutrients at an oyster reef in relation to submarine groundwater discharge. *Science of the Total Environment*, 710, 136283. doi:https://doi.org/10.1016/j.scitotenv.2019.136283

Stets, E.G., Kelly, V.J., and Crawford, C.G. (2014). Long-term trends in alkalinity in large rivers of the conterminous US in relation to acidification, agriculture, and hydrologic modification. *Science of The Total Environment*, 488–489, 280-289.

Swaney, D. P., Humborg, C., Emeis, K., Kannen, A., Silvert, W., Tett, P., et al. (2012). Five critical questions of scale for the coastal zone. *Estuarine, Coastal and Shelf Science, 96*, 9-21.

Twilley, R. R., Cowan, R. J., Miller-Way, T., Montagna, P.A. & Mortazavi, B. (1999). Benthic nutrient fluxes in selected estuaries in the Gulf of Mexico. In: Bianchi, T. S., Pennock, J. R. and R. Twilley (eds.), *Biogeochemistry of Gulf of Mexico Estuaries*, John Wiley & Sons, Inc. pp. 163 - 209.

Van Dam, B. R., Crosswell, J. R., & Paerl, H. W. (2018). Flood-driven CO_2 emissions from adjacent North Carolina estuaries during Hurricane Joaquin (2015). *Marine Chemistry*, *207*, 1-12.

Walker, L. M., Montagna, P.A., Hu, X., Wetz, M.S. (2020). Timescales and magnitude of water quality change in three Texas estuaries induced by passage of Hurricane Harvey. *Estuaries and Coasts*, https://doi.org/10.1007/s12237-020-00846-6

Wang, H., Hu, X., Wetz, M. S., & Hayes, K. C. (2018). Oxygen Consumption and Organic Matter Remineralization in Two Subtropical, Eutrophic Coastal Embayments. *Environ Sci Technol*, *52*(22), 13004-13014.

Wang, S. R., Daniela, D. I., Cai, W.-J., & Hopkinson, C. S. (2017). Inorganic carbon and oxygen dynamics in a marsh-dominated estuary. *Limnology and Oceanography, 63*(1), 47-71.

Wang, Z. A., & Cai, W. J. (2004). Carbon dioxide degassing and inorganic carbon export from a marsh-dominated estuary (the Duplin River): A marsh CO2 pump. *Limnology and Oceanography*, *49*(2), 341-354.

Wang, Z. A., Kroeger, K. D., Ganju, N. K., Gonneea, M. E., & Chu, S. N. (2016). Intertidal salt marshes as an important source of inorganic carbon to the coastal ocean. *Limnology and Oceanography*, *61*(5), 1916-1931.

Weiss, R. F., & Price, B. A. (1980). Nitrous oxide solubility in water and seawater. *Marine Chemistry*, 8, 347-359. doi:10.1016/0304-4203(80)90024-9

Weiss, R. F. (1974). Carbon dioxide in water and seawater: the solubility of a non-ideal gas. *Marine Chemistry, 2*(3), 203-215.

Wetz, M. S., Cira, E. K., Sterba-Boatwright, B., Montagna, P. A., Palmer, T. A., & Hayes, K. C. (2017). Exceptionally high organic nitrogen concentrations in a semi-arid South Texas estuary susceptible to brown tide blooms. *Estuarine, Coastal and Shelf Science, 188*, 27-37.

Willey, J. D., Kieber, R. J., Eyman, M. S., & Avery, G. B. (2000). Rainwater dissolved organic carbon: concentrations and global flux. *Global Biogeochemical Cycles, 14*(1), 139-148.

Windham-Myers, L., Wei Jun, C., Simone, A., Andreas, A., Joseph, C., Kenneth, D., . . . Maria, T. (2018). Chapter 15: Tidal Wetlands and Estuaries. In N. Cavallaro, G. Shrestha, R. Birdsey, M. A. Mayes, R. G. Najjar, S. C. Reed, P. Romero-Lankao, & Z. Zhu (Eds.), *Second State of the Carbon Cycle Report (SOCCR2): A Sustained Assessment Report*. U.S. Global Change Research Program (pp. 596-648). Washington D.C., USA.

Yao, H., & Hu, X. (2017). Responses of carbonate system and CO_2 flux to extended drought and intense flooding in a semiarid subtropical estuary. *Limnology and Oceanography, 62*, S112-S130.

Yao, H., McCutheon, M. R., Staryk, C. J., & Hu, X. (2020). Hydrologic controls on CO_2 chemistry and flux in subtropical lagoonal estuaries of the northwestern Gulf of Mexico. *Limnology and Oceanography*. doi: 10.1002/lno.11394

Yeager, K. M., Santschi, P., Schindler, K., Andres, M., & Weaver, E. (2006). The relative importance of terrestrial versus marine sediment sources to the Nueces-Corpus Christi Estuary, Texas: An isotopic approach. *Estuaries and Coasts, 29*(3), 443-454.

Zeng, F.-W., Masiello, C. A., & Hockaday, W. C. (2011). Controls on the origin and cycling of riverine dissolved inorganic carbon in the Brazos River, Texas. *Biogeochemistry, 104*(1-3), 275-291.

Zhang, J.-Z., & Fischer, C. J. (2014). Carbon Dynamics of Florida Bay: Spatiotemporal Patterns and Biological Control. *Environ Sci Technol, 48*(16), 9161-9169. doi:10.1021/es500510z

Table 1. Hydrologic and sedimentary information for four nwGOM lagoons

Characteristic		Location: LCE	GE	MAE	NE	Reference
Mean Depth (m)		1.1	1.1	1.1	1.2	(Solis & Powell, 1999)
Open Water Area (km^2)		1180.6	561.6	575.7	536.6	(TCEQ)
Watershed Area ($10^3 \cdot km^2$)		130.3	28.1	7.2	45.6	(Montagna et al., 2011)
Residence Time (d)		81	39	360	356	(Bianchi et al., 1999)
Submarine Groundwater Discharge ($m \cdot d^{-1}$)		0.46[a] (0.11)	0.46[1] (0.11)	0.46 (0.11)	1.08 (0.18)	(Murgulet et al., 2018; Spalt et al., 2020)
River Discharge ($m^3 \cdot s^{-1}$)	A	107.9 (137.8)	48.3 (24.8)	7.3 (13.4)	8.6 (16.9)	(USGS, gauge#8162600, 8162000, 8162500, 8164600, 8164800, 8164000, 8188810, 8189800, 8189200, 8189500, 8189700, 8211200, 8211520)
	D	30.0 (16.2)	28.3 (12.0)	0.9 (1.1)	3.0 (1.2)	
	W	273.5 (162.8)	72.5 (16.8)	32.0 (14.4)	23.7 (31.8)	
Average Riverine DIC ($\mu mol \cdot kg^{-1}$)	D	2941.9 (569.6)	4454.9 (535.0)	4948.4 (994.4)	4062.6 (297.4)	(This study)
	W	2061.2 (879.6)	2884.6 (758.5)	2925.7 (957.4)	3744.5 (388.9)	
Average Riverine TOC ($\mu mol \cdot kg^{-1}$)	D	558.4 (204.9)	371.5 (151.4)	300.7 (31.1)	619.3 (72.9)	(TCEQ)
	W	368.7 (242.6)	558.6 (333.4)	777.2 (221.0)	605.9 (125.6)	
Ocean endmember ($\mu mol \cdot kg^{-1}$)	D	DIC	2232.3 (69.6)	TOC	166.7	(TCEQ)
	W	DIC	2094.9 (65.2)	TOC	166.7	
Surface sediment TOC ($mg \cdot C \cdot kg^{-1}$)	D	5.4 (3.7)	6.0 (0.8)	2.8 (0.7)	4.2 (1.8)	(TCEQ)
	W	10.6 (8.1)	9.8 (5.3)	21.4 (15.9)	5.2 (3.3)	
Sediment accumulation Rate[b] ($cm \cdot yr^{-1}$)	Upper	0.79 (0.37)	0.79[c] (0.37)	0.43[c] (0.12)	0.43 (0.12)	(Bronikowski, 2004; Yeager et al., 2006)
	Lower	0.23[c] (0.05)	n/a	0.23[c] (0.05)	0.23 (0.05)	
Bulk density ($g \cdot cm^{-3}$)	For all		2.65			(Bianchi et al., 2013)

Values in bracket indicate the standard deviations.
A=annual average, D=dry condition, including dry and flood relaxation periods, W=wet condition, including flooding and hurricane periods;
TCEQ=Texas Commission of Environmental Quality, Texas Surface Water Quality Monitoring, https://www.tceq.texas.gov/;
[a] assume that SGD in LCE and GE were similar with MAE due to a lack of study;
[b] sediment accumulation rate was based on ^{210}Pb methodology;
[c] assume same sediment accumulation rates for upper LCE/GE, upper MAE/NE, all lower estuarine areas due to lack of study and hydrologic similarities;

Table 2. Error analysis of different carbon budget terms.

Budget Term	Variables	Error
F_{Rv} (DIC)	C_{Rv}, V_{Rv}	C_{Rv}— stand deviation of observations, between estuaries assigned 8.6 – 20.8% for dry condition, 14.5 – 41.5% for wet condition; V_{Rv}—cumulative daily-mean data of each month from USGS.
F_{Rv} (TOC)	C_{Rv}, V_{Rv}	C_{Rv}— stand deviation of historical TCEQ data, between estuaries assigned 14.6 – 55.4% for dry condition, 14.8 – 52.8% for wet condition; V_{Rv}—cumulative daily-mean data of each month from USGS.
F_{CO2}	k, $pCO_{2,\text{water}}$, $pCO_{2,\text{air}}$	k–assigned 20 – 25% for parameterization (Ho et al. 2014); $pCO_{2,\text{water}}$–stand deviation of each field campaign observations; $pCO_{2,\text{air}}$–direct observation from northern Gulf of Mexico region.
F_{NEM}	F_{CO2}	F_{CO2} error propagation; approximately 26.8% difference applied to lagoonal estuary (Laruelle et al., 2013).
F_D	S_a, C_{sed}	S_a–100% due to spatiotemporal variability and lack of study; C_{sed}–stand deviation of historical TCEQ data, between estuaries assigned 12.5 – 28.8% for dry condition, 10.4 – 42.6% for wet condition.
F_{Ex} (DIC and TOC)	V_{Rv}, V_{SGD}, τ, $\overline{C}$, C_{Ocean}	V_{Rv}—cumulative daily-mean data of each month from USGS; V_{SGD}—100% due to spatiotemporal variability and lack of study; τ—referenced residence time; $\overline{C}$— stand deviation of each field campaign observations; C_{Ocean}— stand deviation of contemporary TCEQ data, assigned 3% for both dry and wet conditions.
F_L (DIC and TOC)	Calculated as residual	Error propagation from all other fluxes.

100% error was assigned if estimated with low confidence.

Table 3. Lateral TOC and DIC exchanges from saltmarsh and mangrove (*units*: $mol{\cdot}C{\cdot}m^{-2}{\cdot}yr^{-1}$).

Region	Wetland System	Lateral TOC	Lateral DIC	Reference
Global	Mangrove	21.0 (23.1)	-	(Bouillon et al., 2008)
Global	Mangrove	-	18.7	(Borges et al., 2005)
U.S. East Coast	Salt Marsh	14.9	34.6	(Wang et al., 2016)
U.S. East Coast	Salt Marsh and Mangrove	15.4 (5.9)		(Herrmann et al., 2015)
U.S. East Coast	Salt Marsh And Mangrove		19.6 (10.0)	(Najjar et al., 2018)
Australian East Coast	Mangrove	20.0 (4.7)	34.2 (12.0)	(Maher et al., 2018)
Australian Coast	Mangrove	-	21.5 (10.6)	(Sippo et al., 2016)
Georgia Coast (U.S.)	Salt Marsh	-	13	(Wang & Cai, 2004)
Georgia Coast (U.S.)	Salt Marsh	36.5	-	(Chalmers et al., 1985)
Northwest GOM (U.S.)	Salt Marsh and Mangrove	32.3(4.1)	27.0 (5.3)	This study

Values in bracket indicate the standard deviations.

Table 4. Estuarine carbonate system components (*units*: *$\mu mol \cdot kg^{-1}$ for DIC*) in different hydrologic periods.

Hydrologic condition and corresponding time period		LCE			GE			MAE			NE		
		Sal	pH	DIC	Sal	pH	DIC	Sal	pH	DIC	Sal	pH	DIC
D	April 2014−March 2015; February−August 2017; January−April 2018	24.9 (4.7)	8.103 (0.166)	2314.7 (374.5)	20.7 (7.1)	8.224 (0.215)	2369.3 (285.2)	29.0 (7.3)	8.057 (0.117)	2279.2 (192.6)	34.4 (3.3)	8.031 (0.110)	2264.0 (127.9)
FR	August 2015−May 2016; September 2016−January 2017; September–December 2017	19.9 (4.7)	8.146 (0.114)	2333.8 (345.6)	13.3 (5.2)	8.165 (0.995)	2527.7 (419.0)	20.6 (6.4)	8.162 (0.143)	2342.7 (208.9)	29.9 (1.9)	8.075 (0.102)	2272.2 (120.4)
F	April−July 2015; June−August 2016;	13.4 (8.7)	8.097 (0.307)	2020.7 (414.2)	6.1 (5.4)	8.189 (0.216)	2967.7 (313.1)	14.9 (9.7)	8.210 (0.167)	2110.3 (289.2)	28.2 (4.7)	8.149 (0.173)	2232.9 (221.8)
H	September–October 2017	13.5 (6.2)	8.000 (0.140)	2468.9 (448.8)	6.9 (6.5)	7.896 (0.280)	2293.6 (336.2)	11.6 (5.7)	8.165 (0.163)	1998.4 (220.6)	30.3 (2.3)	8.123 (0.078)	2059 (57.9)

D=drought; FS=flood relaxation; F=flooding; H=hurricane, hydrologic conditions are based on the quartiles of mean salinity, except hurricane period;
Drought and flood relaxation belong to dry condition, flooding and hurricane belong to wet condition;
Values in bracket indicate the standard deviations.

Table 5. Synthesis of observed air-water CO_2 fluxes from North American Coast (*units*: $mol \cdot C \cdot m^{-2} \cdot yr^{-1}$).

Region	MARCATS[a] Segment No.	Number of Systems	Average air-water CO_2 flux[b] ($mol \cdot C \cdot m^{-2} \cdot y^{-1}$)
High Latitude of Pacific Coast	1	3	2.0 (5.5)
Pacific Coast	2	1	0.4
Gulf of Mexico	9	7	15.7 (16.4)
Atlantic Coast	10	11	6.5 (6.2)
High Latitude of Atlantic Coast	11	1	0.5
High Latitude	12	1	-0.4
Total		26	7.5 (10.9)

[a] MARCATS segmentation numbers were based on Laruelle et al., 2013.
[b] average CO_2 flux was calculated as arithmetic mean of integrated estuarine observations, see details in Table S2.

Figure 1.


a
Gulf of Mexico
Texas
Lavaca-Colorado Estuary (LCE)
Guadalupe Estuary (GE)
Mission-Aransas Estuary (MAE)
Nueces Estuary (NE)
Gulf of Mexico
Lavaca River
Tres Palacios River
Colorado River
Guadalupe River
San Antonio River
Mission River
Aransas River
Nueces River
Oso Creek
98° W
97° W
96° W
28° N
N
0 20 40 Kilometers
b
Riverine DIC sampling station
Estuarine Sampling Stations
c
TCEQ riverine TOC station
NOAA weather station
USGS river gauge
d
Literature sedimentation station
TCEQ sediment TOC station

Figure 2.

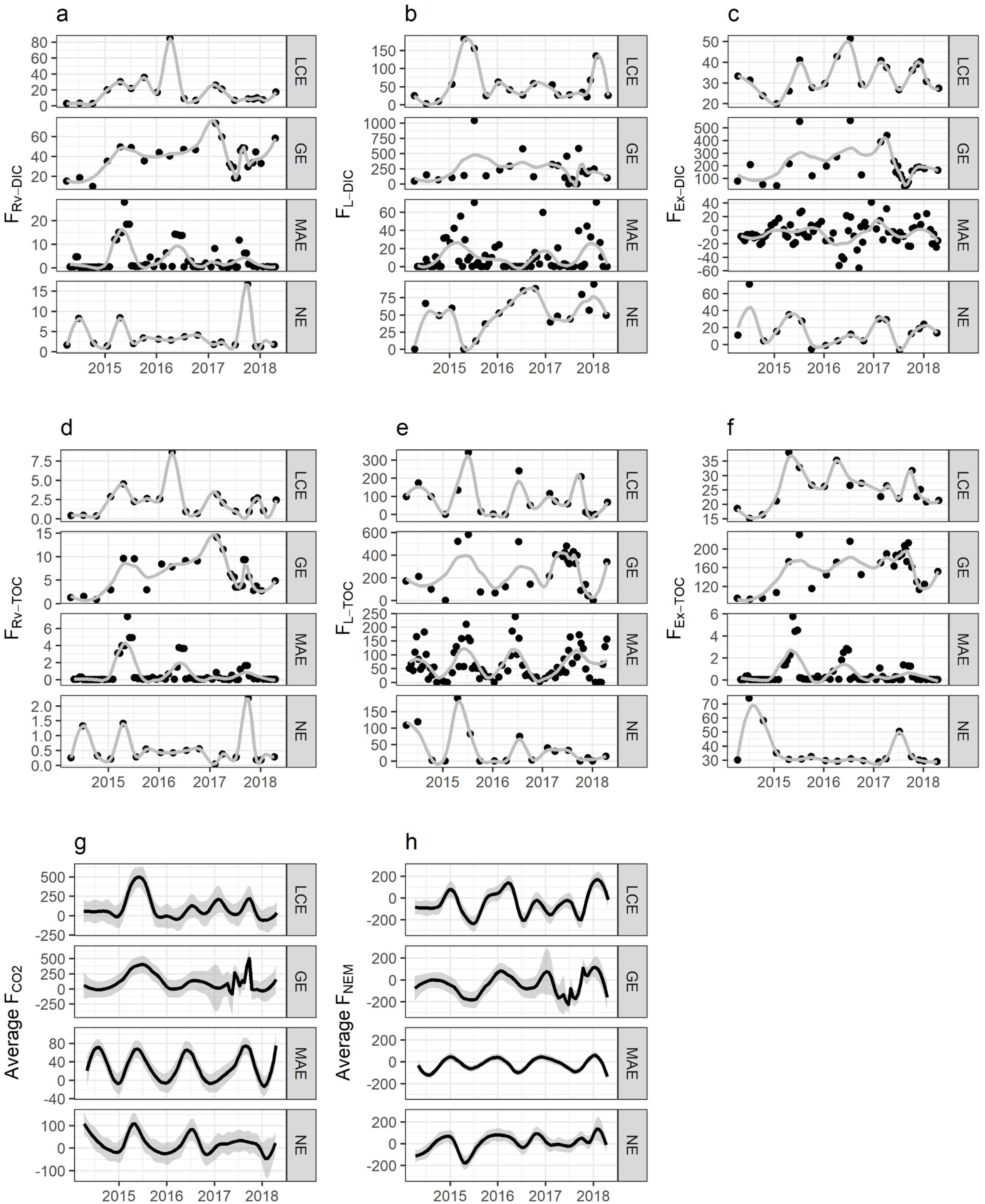

a
b
c
d
e
f
g
h
F Rv−DIC
F L−DIC
F Ex−DIC
F Rv−TOC
F L−TOC
F Ex−TOC
Average F CO2
Average F NEM
LCE
GE
MAE
NE
2015
2016
2017
2018

Figure 3.

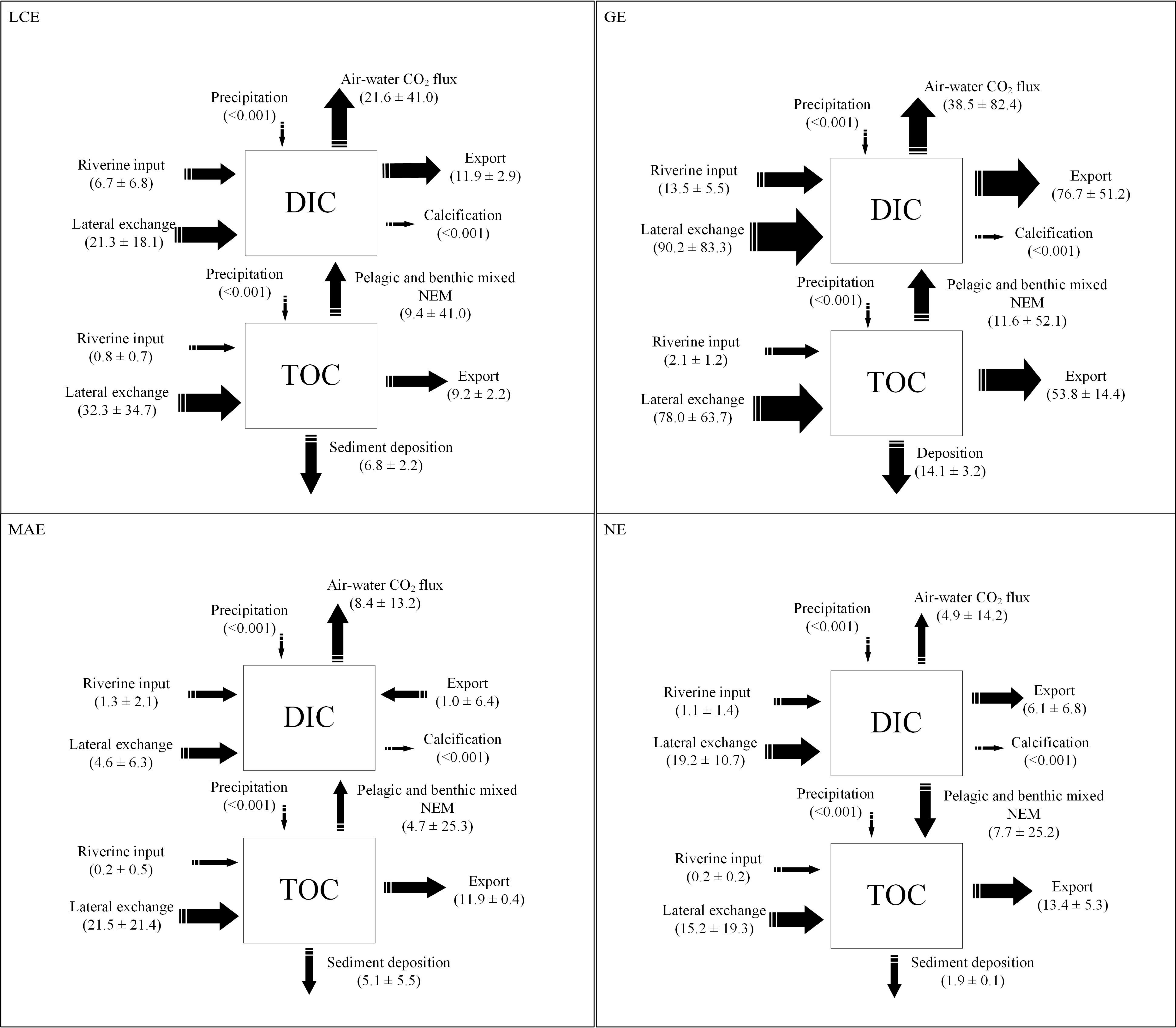
LCE
Precipitation
(<0.001)
Air-water CO2 flux
(21.6 ± 41.0)
Riverine input
(6.7 ± 6.8)
DIC
Export
(11.9 ± 2.9)
Lateral exchange
(21.3 ± 18.1)
Calcification
(<0.001)
Precipitation
(<0.001)
Pelagic and benthic mixed
NEM
(9.4 ± 41.0)
Riverine input
(0.8 ± 0.7)
TOC
Export
(9.2 ± 2.2)
Lateral exchange
(32.3 ± 34.7)
Sediment deposition
(6.8 ± 2.2)
GE
Precipitation
(<0.001)
Air-water CO2 flux
(38.5 ± 82.4)
Riverine input
(13.5 ± 5.5)
DIC
Export
(76.7 ± 51.2)
Lateral exchange
(90.2 ± 83.3)
Calcification
(<0.001)
Precipitation
(<0.001)
Pelagic and benthic mixed
NEM
(11.6 ± 52.1)
Riverine input
(2.1 ± 1.2)
TOC
Export
(53.8 ± 14.4)
Lateral exchange
(78.0 ± 63.7)
Deposition
(14.1 ± 3.2)
MAE
Precipitation
(<0.001)
Air-water CO2 flux
(8.4 ± 13.2)
Riverine input
(1.3 ± 2.1)
DIC
Export
(1.0 ± 6.4)
Lateral exchange
(4.6 ± 6.3)
Calcification
(<0.001)
Precipitation
(<0.001)
Pelagic and benthic mixed
NEM
(4.7 ± 25.3)
Riverine input
(0.2 ± 0.5)
TOC
Export
(11.9 ± 0.4)
Lateral exchange
(21.5 ± 21.4)
Sediment deposition
(5.1 ± 5.5)
NE
Precipitation
(<0.001)
Air-water CO2 flux
(4.9 ± 14.2)
Riverine input
(1.1 ± 1.4)
DIC
Export
(6.1 ± 6.8)
Lateral exchange
(19.2 ± 10.7)
Calcification
(<0.001)
Precipitation
(<0.001)
Pelagic and benthic mixed
NEM
(7.7 ± 25.2)
Riverine input
(0.2 ± 0.2)
TOC
Export
(13.4 ± 5.3)
Lateral exchange
(15.2 ± 19.3)
Sediment deposition
(1.9 ± 0.1)

Figure 4.

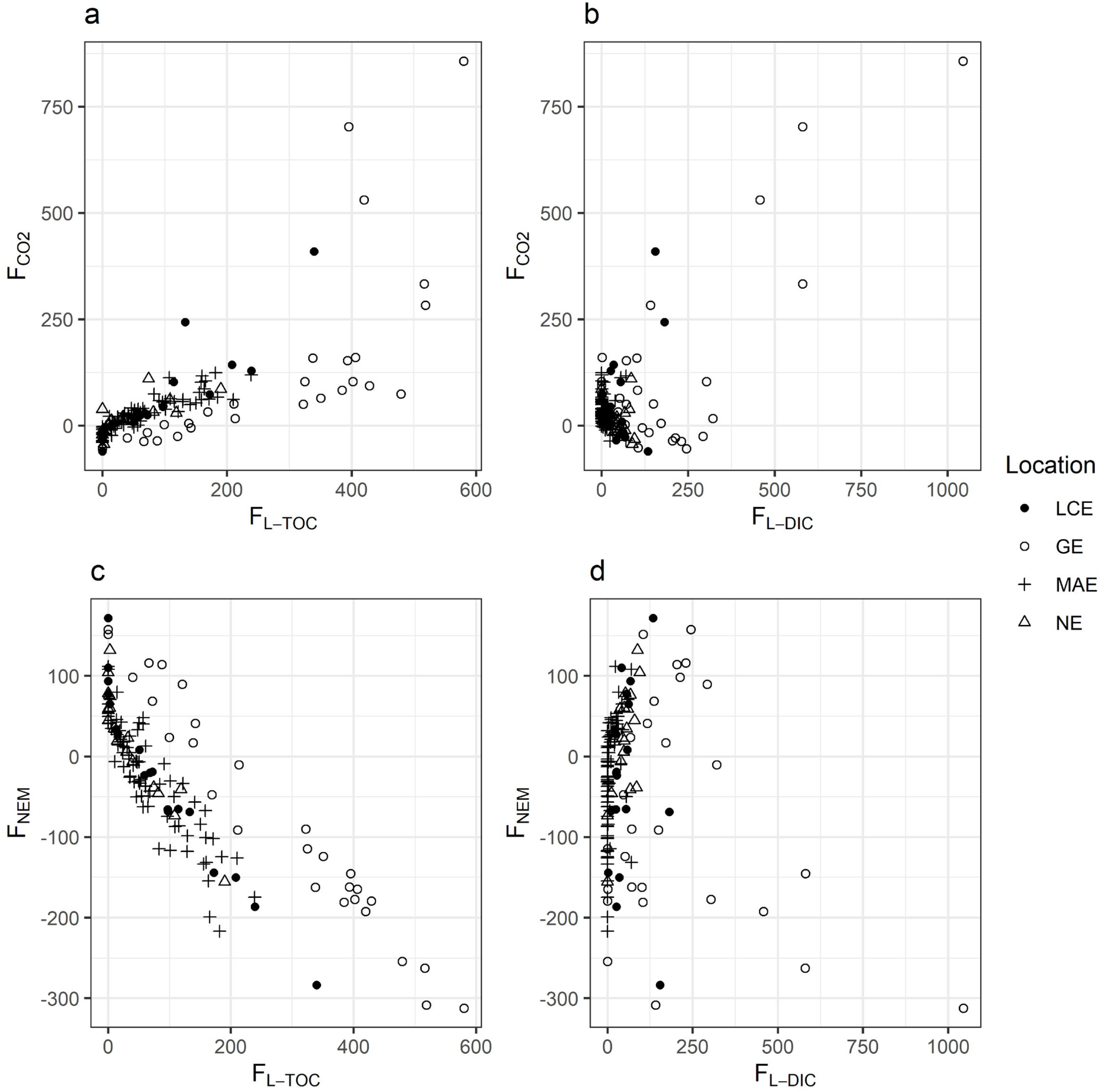

a
b
c
d
F_{CO2}
F_{NEM}
F_{L-TOC}
F_{L-DIC}
750
500
250
0
100
-100
-200
-300
200
400
600
1000
Location
LCE
GE
MAE
NE

Figure 5.

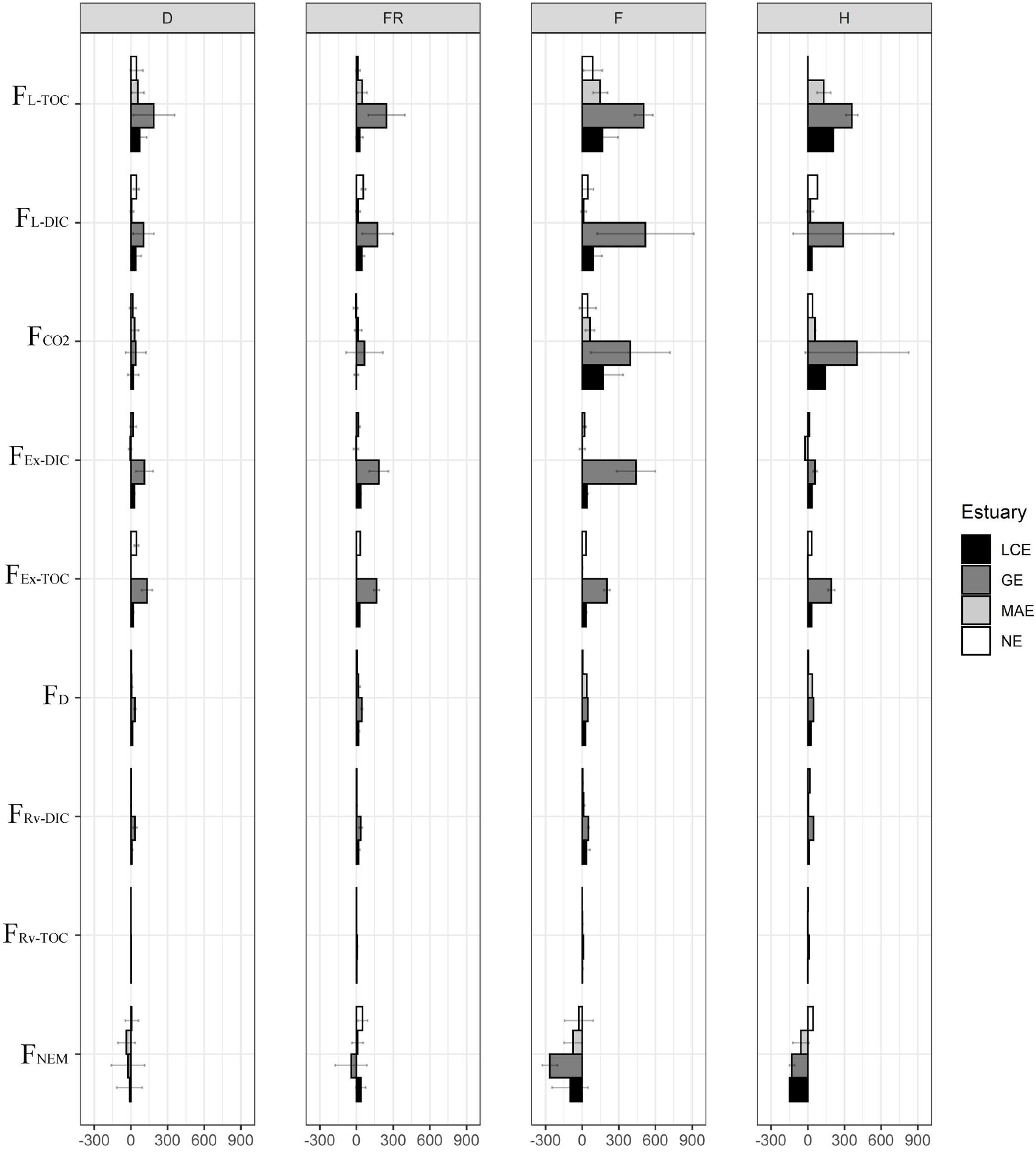

D
FR
F
H
F_{L-TOC}
F_{L-DIC}
F_{CO2}
F_{Ex-DIC}
F_{Ex-TOC}
F_D
F_{Rv-DIC}
F_{Rv-TOC}
F_{NEM}
-300
0
300
600
900
Estuary
LCE
GE
MAE
NE

Figure 6.

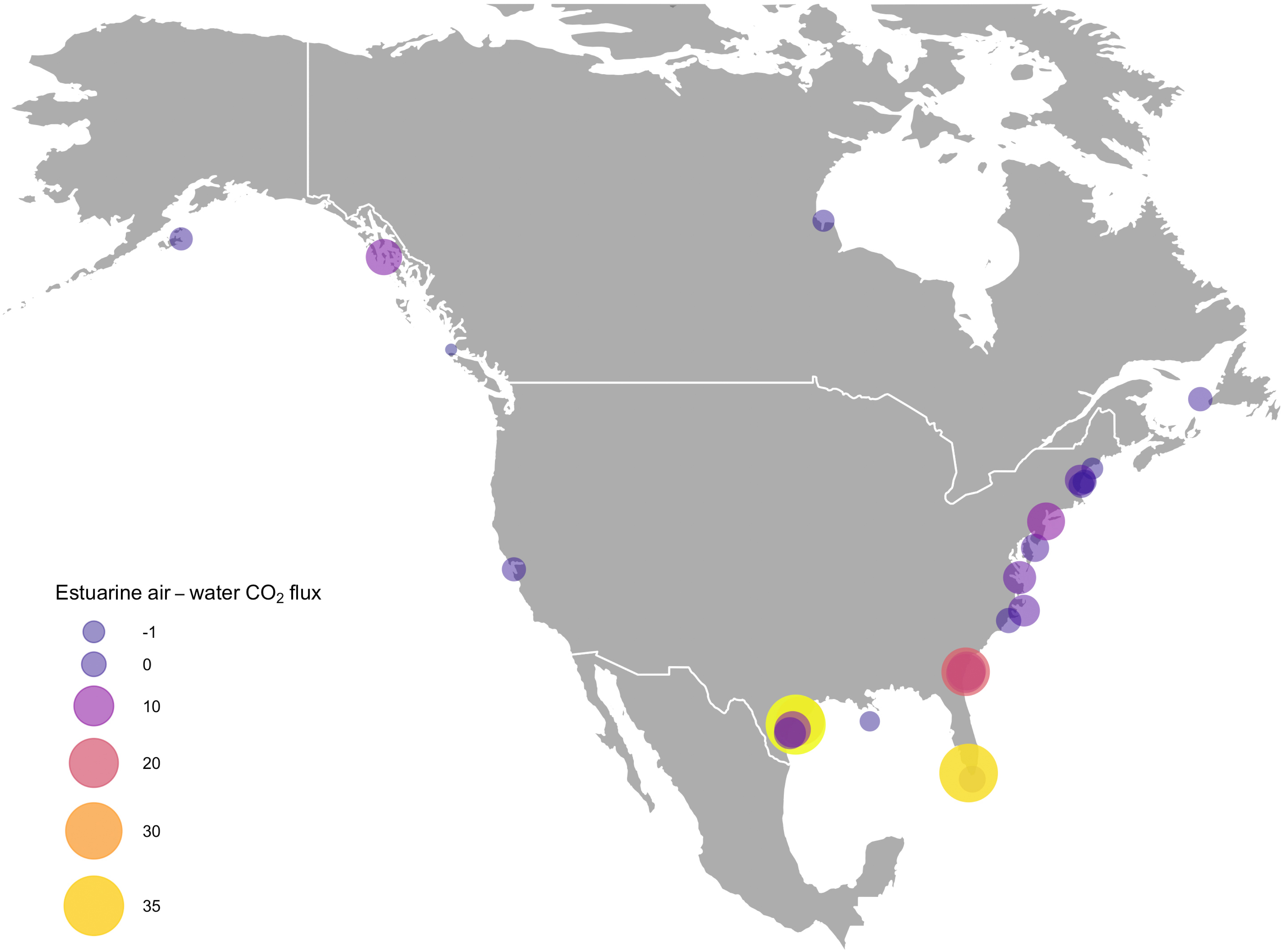
Estuarine air – water CO_2 flux
-1
0
10
20
30
35

Figure 7.

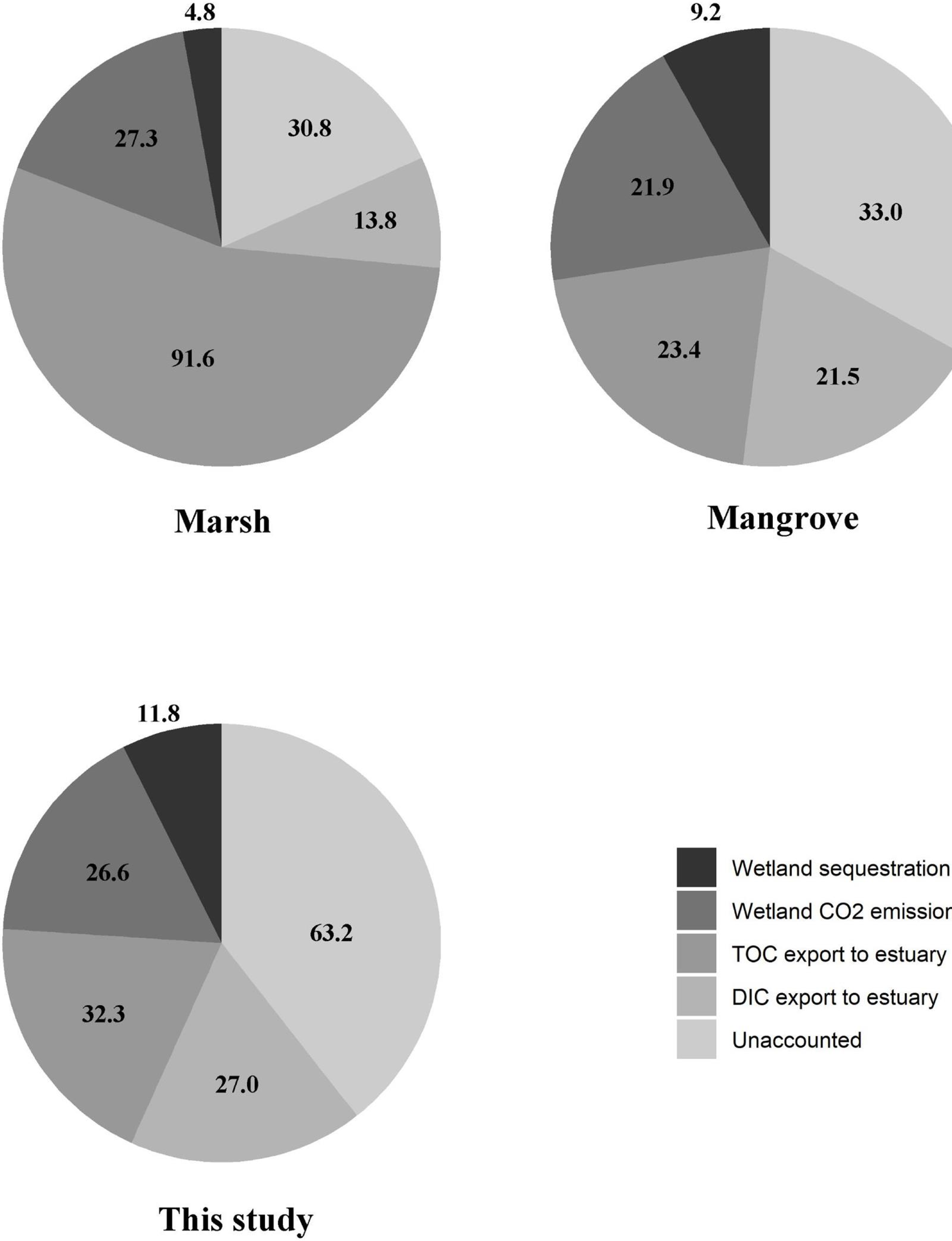
4.8
30.8
27.3
13.8
91.6
Marsh
9.2
21.9
33.0
23.4
21.5
Mangrove
11.8
26.6
63.2
32.3
27.0
This study
Wetland sequestration
Wetland CO2 emission
TOC export to estuary
DIC export to estuary
Unaccounted

Figure 8.


River
(a) 5.0 ± 1.1
(b) 0.7 ± 0.1
(e) 16.8 ± 3.0
(h) 17.0 ± 5.2
(i) 17.6 ± 2.5
(j) ~160.3
(k) ~26.6
DIC
(f) 4.4 ± 2.2
Ocean
(c) 27.0 ± 5.3
(d) 32.3 ± 4.1
TOC
(g) 6.3 ± 0.9
Marshes and Mangroves
Sediment
(l) ~5.0